ACCSCIENCE PUBLISHING

Advanced Neurology

ORIGINAL RESEARCH ARTICLE

Mechanistic investigation of *Xijiao Dihuang* decoction for ischemic stroke: A network pharmacology and *in vivo* validation study

Qiuhua He, Fantao Song, Yujie Wang, and Zhaoyao Chen*

Department of Neurology, Jiangsu Province Hospital of Chinese Medicine, Affiliated Hospital of Nanjing University of Chinese Medicine, Nanjing, Jiangsu, China

Abstract

Ischemic stroke is the most prevalent and severe form of cerebrovascular disease and a leading cause of significant neurological disability. As the primary cause of hospitalization for neurological disorders, it necessitates urgent and effective therapeutic interventions. *Xijiao Dihuang* decoction (XJDHT), a classical traditional Chinese medicinal formula, is traditionally known for its effects in heat clearing, detoxification, blood cooling, and blood stasis removing. Emerging evidence suggests its potential to promote neurological recovery following ischemic stroke; however, systematic evaluation remains limited. This study employed a systematic network pharmacology approach to elucidate the molecular mechanisms underlying XJDHT's therapeutic effects on ischemic stroke. LC-MS identified 24 bioactive compounds in XJDHT, using Traditional Chinese Medicine Systems Pharmacology and SwissTargetPrediction databases for target prediction. Disease targets for ischemic stroke were retrieved from GeneCards, Online Mendelian Inheritance in Man, Therapeutic Target Database, and Gene Expression Omnibus datasets. Intersection analysis found 424 overlapping targets between 690 compound targets and 3415 disease targets. Cytoscape and STRING platforms were used to construct networks and identify hub genes and critical modules. Functional enrichment analysis was conducted using the Database for Annotation, Visualization, and Integrated Discovery database. Network analysis identified core bioactive constituents, including paeoniflorin, albiflorin, benzoylpaeoniflorin, kaempferol, paeonol, ellagic acid, pinostrobin, β-sitosterol, and stigmasterol. Key therapeutic targets comprised phosphatidylinositol-4,5-bisphosphate 3-kinase regulatory subunit 1, SRC proto-oncogene, signal transducer and activator of transcription 3, phosphatidylinositol-4,5-bisphosphate 3-kinase catalytic subunit alpha, phosphatidylinositol-4,5-bisphosphate 3-kinase catalytic subunit beta, phosphatidylinositol-4,5-bisphosphate 3-kinase catalytic subunit delta, AKT serine/threonine kinase 1, epidermal growth factor receptor, estrogen receptor 1, Harvey rat sarcoma virus, and neuroblastoma RAS viral oncogene homolog. The Kyoto Encyclopedia of Genes and Genomes pathway enrichment revealed significant involvement in the mammalian target of rapamycin signaling pathway, mitogen-activated protein kinase cascade, phosphatidylinositol 3-Kinase-Protein Kinase B (PI3K-AKT) pathway, erythroblastic leukemia viral oncogene homolog signaling, and vascular endothelial growth factor-mediated angiogenesis. These findings suggest XJDHT exerts neuroprotective effects through coordinated modulation of inflammatory responses and cellular signaling cascades, exhibiting the characteristic therapeutic properties of a multicomponent, multitarget, and multipathway approach.

Keywords: Ischemic stroke; Traditional Chinese medicine; Network pharmacology; Micromolecular protein; Anti-inflammation; Antioxidation

***Corresponding author:**
Zhaoyao Chen
(neurozy@vip.163.com)

Citation: He Q, Song F, Wang Y, Chen Z. Mechanistic investigation of *Xijiao Dihuang* decoction for ischemic stroke: A network pharmacology and *in vivo* validation study. *Adv Neurol.* 2026;5(1):56-79. doi: 10.36922/AN025100020

Received: March 4, 2025

1st revised: April 30, 2025

2nd revised: May 23, 2025

Accepted: June 9, 2025

Published online: July 4, 2025

1. Introduction

Ischemic stroke, resulting from cerebral artery occlusion, constitutes one of the leading causes of chronic neurological disability worldwide. Despite the progress made in medical science, the development of effective therapeutic interventions to enhance functional recovery post-stroke remains an unmet clinical need with a significant socioeconomic burden.[1] Stroke management has entered a dynamic era of innovation, with current therapeutic paradigms revolutionized by two groundbreaking interventions: Intravenous thrombolysis and endovascular mechanical thrombectomy.[2] Additional strategies include antiplatelet aggregation therapy, lipid-lowering interventions, plaque stabilization, and comprehensive management of underlying conditions such as atrial fibrillation, hypertension, and diabetes mellitus.

According to traditional Chinese medicine (TCM) theory, the pathogenesis of stroke originates from the accumulation of endogenous pathogenic factors, including internal trauma, emotional overstimulation, improper diet, and chronic fatigue. These factors can lead to hepatic *Yang* hyperactivity, phlegm-heat retention, or *qi* deficiency with phlegm-dampness accumulation, ultimately causing disruption of wind regulation, imbalance of *qi*-blood circulation, and dysfunction of the meridian networks. This pathophysiological cascade contributes to cerebrovascular impairment through blood stasis or hemorrhagic extravasation.

Xijiao Dihuang decoction (XJDHT), a classical formula documented in the Tang Dynasty medical compendium *Medical Secrets of an Official* by Wang Tao, exhibits dual therapeutic effects: Heat clearing/detoxification and blood cooling/stasis dispelling. Studies have demonstrated that XJDHT promotes the proliferation, migration, and tube formation of endothelial cells by upregulating vascular endothelial growth factor (VEGF) and basic fibroblast growth factor, which together stimulate the release of matrix-degrading enzymes from endothelial cells, enhance cell migration ability, and promote neovascularization. Concurrently, XJDHT alleviates inflammatory responses associated with ischemic brain injury by inhibiting proinflammatory factors, thereby improving neurological deficits.[3] In addition to promoting vascular endothelial growth and exerting anti-inflammatory effects, XJDHT enhances the proliferation and differentiation of neural stem cells by upregulating glial cell line-derived neurotrophic factor and brain-derived neurotrophic factor in middle cerebral artery occlusion (MCAO) rats, thereby supporting endogenous neural repair.[4] At the molecular level, XJDHT plays a neuroprotective role by inhibiting Toll-like receptor 4/myeloid differentiation factor 88/nuclear factor kappa-light-chain-enhancer of activated B cells (NF-κB) signaling pathway, which alleviates oxygen-glucose deprivation/reperfusion-induced inflammatory response and neuronal apoptosis.[5] Although research has demonstrated the neuroprotective, anti-inflammatory, and neural repair-promoting properties of XJDHT, its material basis underlying XJDHT's therapeutic effects and precise molecular remain inadequately characterized. To address this gap, the present study employed a network pharmacology approach to explore the mechanisms by which XJDHT facilitates neurological recovery.

Network pharmacology, grounded in systems biology principles, enables comprehensive analysis of biological networks and identification of key signaling nodes involved in multitarget drug actions. This discipline emphasizes multipathway regulation to enhance therapeutic efficacy when minimizing side effects, thereby improving clinical success rates and reducing drug development costs. The inherently multitarget nature of TCM formulations aligns well with the holistic and systematic framework network pharmacology, making this methodology particularly suitable for investigating the complex pharmacological mechanisms of Chinese herbal compounds.[6]

2. Materials and methods

2.1. Materials

Male Sprague–Dawley rats weighing 260 – 280 g were purchased from Hangzhou Medical College (SPF-grade, license No. SCXX [Zhe] 2019-0002) and housed in the animal facility of Nanjing Surui Co., Ltd. The facility maintained a temperature of 26 ± 2°C, relative humidity of 55 ± 5%, a 12 h/12 h light/dark cycle, and provided *ad libitum* access to food and water.

The XJDHT sample, consisting of 9 g of *Paeonia lactiflora*, 24 g of *Rehmannia*, 12 g of *Paeonia suffruticosa*, and 30 g of buffalo horn, was analyzed using mass spectrometry to obtain spectra and a composition table. The samples were sourced from the Pharmacy of Chinese Medicine at the First Clinical College of Nanjing University of Chinese Medicine. After decoction and filtration, the combined filtrate was concentrated using a rotary evaporator to achieve a final concentration of 1 g/mL. The resulting extract was stored at 4°C.

The reagents and instruments used in this study included:

(i) Edaravone injection (5 mL: Edaravone 10 mg and d-camphene 2.5 mg; Simcere Pharmaceutical Co., LTD, China);
(ii) 2,3,5-triphenyl-tetrazolium chloride (TTC) staining solution (2%; G3005; Solarbio, China);
(iii) Digital thermostatic water bath (HH-2; Shanghai

Yetuo, China);
(iv) Neuroblastoma RAS viral oncogene homolog (NRAS) polyclonal antibody (50 μL; Polymer Technology Group (PTG), America);
(v) 300 kDa global transcriptional coactivator (p300) antibody (50 μL; Affinity Biosciences, China);
(vi) LightCycler®480 real-time fluorescence quantitative polymerase chain reaction (qPCR) instrument (Roche Diagnostics, Germany);
(vii) RNA extraction reagent (Vazyme, China);
(viii) Reverse transcription (RT) Super Mix (Vazyme, China);
(ix) Fluorophore-conjugated secondary antibodies (Invitrogen, USA);
(x) Fluorescence microscope (Olympus IX71, Japan).

2.2. Model development

Twenty-four male Sprague–Dawley rats (280 – 330 g) were randomly divided into four groups (n = 6 per group): Control group, MCAO group, XJDHT group, and edaravone group. All rats were fasted for 12 h (with free access to water) prior to surgery. Anesthesia was induced via intraperitoneal injection of 10% chloral hydrate (3 mL/kg). The MCAO model was established using Longa's suture method. The anesthetized rats were secured in a supine position on a surgical board. After neck skin disinfection, a midline incision was made, and the muscles and fascia were bluntly dissected along the medial border of the sternocleidomastoid muscle to expose the right common carotid artery (CCA), external carotid artery (ECA), and internal carotid artery (ICA). Sutures were pre-placed at the distal and proximal ends of the CCA and ECA. A microvascular clip was used to temporarily occlude the ICA. The CCA and ECA were ligated proximally, and a small incision was made 4 mm from the CCA bifurcation. A nylon monofilament (marked with correction fluid 19 mm from the tip) was inserted into the ICA and gently advanced using ophthalmic forceps until resistance was felt at the bifurcation of the ICA and ECA. The pre-placed sutures at the distal CCA and ICA were then tightened to secure the filament. After 90 min of ischemia, the filament was slowly withdrawn to initiate reperfusion. The muscle and skin layers were sutured sequentially, followed by iodophor disinfection. Post-operative intragastric administration and intraperitoneal injections were initiated 2 h after full recovery from anesthesia. Drug treatments were administered once daily at fixed intervals from post-operative days 2 – 7. On the 7th post-operative day, 2 h after administration, blood was collected under anesthesia, and the animals were sacrificed for brain collection. The brains of two mice in each group were fixed with 4% paraformaldehyde. The two rat brains were frozen at -80°C. The remaining brains were quickly harvested and transferred in a phosphate-buffered saline (PBS) solution at 0 - 4°C, then frozen in a refrigerator at -20°C for 30 min. The cerebellum, olfactory bulb, and lower brainstem were removed, and 2 mm-thick coronal brain slices were prepared. The slices were placed in appropriately sized containers, and TTC staining solution was added to completely immerse the tissue. The containers were incubated in water at 37°C in the dark for 20 – 30 min, with gentle shaking every 5 min to ensure thorough staining. After staining, the brain slices were rinsed with PBS solution for 3 – 5 min and then placed on a suitable background plate for photography and observation. Following photography, the slices were fixed in 4% paraformaldehyde. Brain slices from the control group appeared red, with no visible white infarcted area. Normal areas were stained red, while infarcted areas appeared white.

2.3. Determination of XJDHT composition

A compound library was established based on relevant literature and information on chemical compositions found in medicinal materials. Peakview SoftwareTM (AB Sciex) software was utilized for data analysis by inputting chemical formulas and molecular weight information. By combining secondary information fragments obtained from mass spectrometry with reference substances, compound databases, and related literature reports as references, the chemical compositions and structures of the compound preparations were further confirmed. Chromatograms derived from Peakview data were generated using Origin Pro 8.0 software to create a compound composition table for XJDHT.

2.4. XJDHT effective component selection

The Traditional Chinese Medicine Systems Pharmacology (TCMSP) database (https://tcmsp.91medicine.cn) and SwissADME database (http://www.swissadme.ch) were employed for pharmacochemical analysis, with a specific focus on oral bioavailability (OB), a critical pharmacokinetic parameter quantifying the rate and extent of systemic absorption. Potential bioactive compounds in the TCMSP database were systematically screened using stringent criteria: OB ≥ 30% and drug-likeness (DL) ≥0.18. Structural information for each compound was retrieved from the UniProt database (http://www.uniprot.org/uniprot/). Chemical identifiers from TCMSP were cross-referenced with SwissADME entries to obtain comprehensive molecular descriptors. Gastrointestinal (GI) absorption was evaluated as the percentage of compound absorption through intestinal epithelium, whereas blood–brain barrier (BBB) permeability was

categorized as positive or negative based on predictive models. SwissADME's five DL evaluation frameworks (Lipinski's, Ghose's, Veber's, Egan's, and Muegge's rules) were applied concurrently. For inclusion criteria, compounds were required to simultaneously satisfy: (i) High GI absorption classification, (ii) positive BBB permeability prediction, and (iii) compliance with all five established DL rules.

2.5. Active ingredients and disease targets screening

The chemical composition of the selected medicinal inputs was systematically obtained from two authoritative pharmacological databases: The SwissTargetPrediction target database (http://swisstargetprediction.ch) and the TCMSP database. These sources were cross-referenced to identify bioactive components meeting established target screening criteria. Subsequently, disease-associated genetic targets for ischemic stroke were comprehensively retrieved through multidatabase interrogation, including GeneCards (https://www.genecards.org/), Online Mendelian Inheritance in Man (OMIM, https://www.omim.org), and the Gene Expression Omnibus (GEO, https://www.ncbi.nlm.nih.gov/geo/), with strict inclusion parameters limited to experimentally validated human genes. Following duplicate removal and data consolidation, a curated set of ischemic stroke-related therapeutic targets was established. Intersectional analysis employing a Venn diagram methodology revealed statistically significant overlaps between pharmacologically active components and pathological targets, thereby identifying putative key molecular targets for TCM-based therapeutic intervention in ischemic stroke management.

2.6. Core target screening and analysis of the protein–protein interaction (PPI) network

PPI network construction and network topology analysis were performed using the STRING platform (https://cn.string-db.org/). Intersecting genes in *Homo sapiens* were identified with a confidence threshold set at 0.900 to ensure high-quality interactions, excluding unconnected gene nodes. The resulting protein interaction data were imported into Cytoscape 3.10.2 software, and network topology parameters were obtained using the "Network Analyzer" tool. The degree value represents the significance of each target, with higher values indicating greater importance of both drugs and targets. Core targets were ranked based on their degree values.

2.7. Gene Ontology (GO) and Kyoto Encyclopedia of Genes and Genomes (KEGG) enrichment analysis

GO and KEGG enrichment analyses were conducted using the Database for Annotation, Visualization, and Integrated Discovery (DAVID; https://david.ncifcrf.gov/). GO analysis employed a standardized ontological framework to systematically characterize target proteins across three hierarchical domains: Biological processes (BP), cellular components (CC), and molecular functions (MF). BP annotations encompassed drug treatment-related cellular activities, including proliferation regulation, signal transduction cascades, and metabolic pathways. CC annotations identified subcellular localization patterns, whereas MF annotations delineated molecular-level interactions and catalytic activities. Simultaneously, KEGG pathway analysis was performed to identify key signaling pathways associated with therapeutic mechanisms. The top 20 significantly enriched terms from each ontological category (BP, CC, and MF) and KEGG pathways were selected based on hypergeometric test p-values (<0.05). Visualization of the enrichment results, including multidimensional bubble charts and comparative histograms, was conducted using the Bioinformatics.com.cn platform (https://www.bioinformatics.com.cn/). This analytical approach enabled the comprehensive mapping of drug–target interactions to fundamental BP and disease-relevant signaling networks.

2.8. KEGG pathway filtering based on literature review

The present study systematically investigated molecular mechanisms in human biological pathways by querying 20 KEGG pathways through the KEGG database (https://www.kegg.jp/kegg/kegg1.html). Pathway selection criteria were established through a two-phase process: Initial prioritization of stroke-related terms via PubMed database searches (https://pubmed.ncbi.nlm.nih.gov/), followed by comprehensive analysis of existing literature to identify validated signaling pathways, protein interactions, and pathway crosstalk. Identified molecular components were subsequently re-examined in the KEGG database to map upstream–downstream regulatory relationships. Proteins demonstrating significant associations with active ingredient–disease interactions were prioritized for molecular docking simulations and experimental validation through rigorous selection protocols.

2.9. Messenger RNA transcript level quantification via quantitative real-time polymerase chain reaction

Real-time qPCR is a method that uses fluorescent chemicals to measure the total amount of product after each PCR cycle in a DNA amplification reaction. It allows for quantitative analysis of a specific DNA sequence in a test sample using internal or external reference standards. The messenger RNA (mRNA) expression level indirectly reflects potential protein synthesis. Proteins with significantly altered

mRNA transcription levels in the XJDHT group were selected for molecular docking and immunofluorescence staining. The specific steps were as follows: After cell lysis, 50 μL p300 antibody and 50 μL NRAS antibody were prepared. For sample processing and antibody premixing, a total RNA extraction reagent was used to extract mRNA from rat brain tissue. Complementary DNA (cDNA) was synthesized by reverse transcription using RT Super Mix to quantify the mRNA levels of each factor. PCR analysis of the diluted cDNA samples was performed using Fluorescent Quantitative PCR Mix and the LightCycler®480 II system.

2.10. Molecular docking

Molecular docking simulates the molecular recognition process between small-molecule ligands and macromolecular protein targets, with binding energy (affinity) serving as the primary quantitative metric for evaluating docking performance. Lower binding energy values indicate more favorable molecular interactions and more stable complex formation.

The experimental protocol comprised three principal phases: Ligand preparation, protein preparation, and docking implementation. Ligand structures of bioactive compounds were retrieved from PubChem (https://pubchem.ncbi.nlm.nih.gov/) in Semantic Definition Format, followed by molecular optimization using PyMOL software for hydrogen atom addition and charge assignment employing the MMFF94 force field. Energy minimization procedures were subsequently performed to achieve stable molecular conformations, with final conversion to PDBQT format executed through AutoDockTools. Protein target selection from the RCSB Protein Data Bank (http://www.rcsb.org/) adhered to three critical criteria: (i) Biological relevance in disease pathology; (ii) presence of cocrystallized ligands; and (iii) preferential selection of crystal structures with minimized resolution values. Protein preparation involved ligand separation, hydrogen addition, and charge calculation via AutoDockTools, culminating in conversion to PDBQT format. Docking parameters were standardized using AutoDockTools to define grid box dimensions and coordinate centering. Molecular docking simulations were performed using AutoDock Vina, followed by affinity extraction and statistical analysis of binding energies for comparative evaluation.

2.11. Immunofluorescence staining

Immunofluorescence staining is a laboratory technique used to identify and localize specific biomolecules within cellular or tissue specimens through the utilization of fluorophore-conjugated antibodies, which exhibit high affinity for target epitopes, enabling precise spatial visualization through fluorescence microscopy. Proteins demonstrating significant expression alterations in qPCR analyses were subjected to immunofluorescence localization in rat cerebral tissue sections using Alexa Fluor 594-conjugated secondary antibodies. Confocal laser scanning microscopy facilitated detailed observation of protein distribution patterns within neuroanatomical structures. Quantitative fluorescence intensity measurements were acquired through standardized threshold analysis in ImageJ software (v1.53t; National Institutes of Health, US), with statistical data presented in comparative histogram format. Paraffin-embedded brain tissue sections were deparaffinized and rehydrated through graded alcohols, then fixed in 4% paraformaldehyde. Sections were permeabilized with 0.3% Triton X-100 for 5 min and blocked with bovine serum albumin for 30 min at room temperature to reduce non-specific binding. Subsequently, sections were incubated overnight at 4°C with primary antibodies against E1A binding protein P300 (EP300) and NRAS. After washing, sections were incubated with appropriate fluorophore-conjugated secondary antibodies (Invitrogen, USA) for 30 min at room temperature. Nuclear counterstaining was performed using 4',6-diamidino-2-phenylindole. Immunofluorescent signals for EP300 and NRAS were visualized using a fluorescence microscope (Olympus IX71, Japan) under appropriate filter settings.

3. Results

3.1. Observation of curative effect

As illustrated in Figure 1, rat brain tissue sections are categorized into four groups: (i) Control group, (ii) MCAO model group, (iii) XJDHT treatment group, and (iv) edaravone positive control group (abbreviated as edaravone). After treatment with XJDHT and edaravone, the area of white infarction was reduced. Table 1 presents the volume ratio of ischemic regions in brain tissue for each group. The volume ratio of the ischemic area was highest in the MCAO group, indicating successful model establishment. Blocking the middle cerebral artery blood flow in rats led to obvious ischemic cerebral infarction. The volume ratios in the XJDHT group were 22.40 and 10.64; notably, the value of 10.64 was much lower than that in the MCAO group, suggesting that XJDHT treatment has the potential to improve ischemia. In terms of efficacy, XJDHT appears to be superior to edaravone. Brain slices from the control group appeared red, with no visible white infarction areas. According to the TTC staining results, the proportion of infarction area to the total brain area was highest in the MCAO model group compared to the control group, while the proportions were significantly reduced in the XJDHT decoction and edaravone groups.

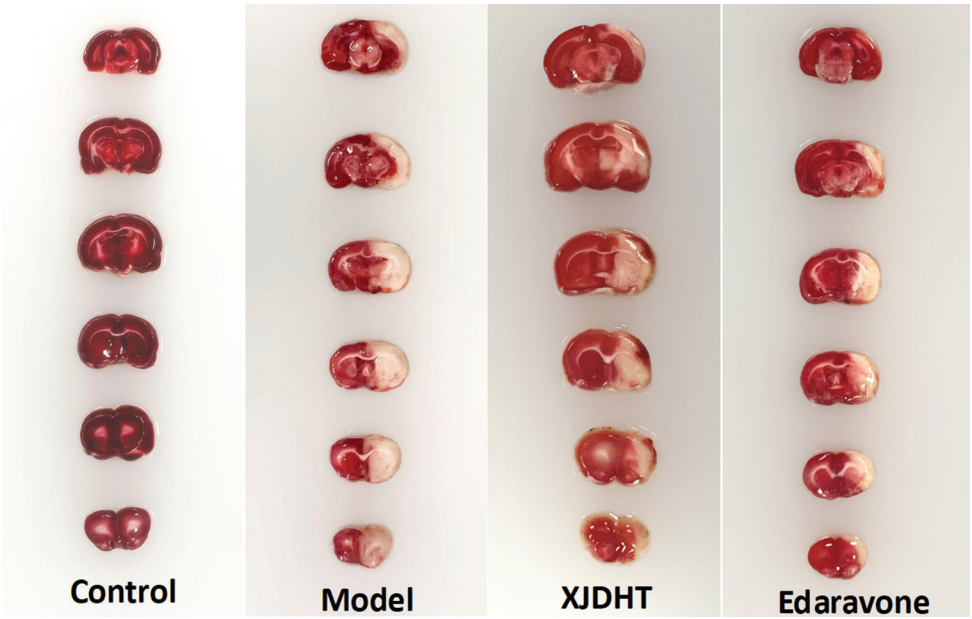

Figure 1. Schematic representation of the ischemic regions in rat brain tissue following treatment with each reagent
Abbreviation: XJDHT: *Xijiao Dihuang* decoction.

Table 1. Volume ratio of ischemic areas across groups

Group	Volume ratio of ischemic zone (%)	Mean value
1. Control	0	0
	0	
2. MCAO	33.94050568	36.80571236
	39.67091903	
3. Edaravone	13.31372863	17.03825104*
	20.76277344	
4. XJDHT	22.40604662	16.52421605*
	10.64238547	

Note: *$p<0.05$.
Abbreviations: MCAO: Middle cerebral artery occlusion; XJDHT: *Xijiao Dihuang* decoction.

3.2. Determination of drug components in XJDHT

Under optimized ultra-performance liquid chromatography coupled with quadrupole time-of-flight mass spectrometry conditions, representative ion chromatograms were obtained to define chromatographic separation parameters. The characteristic ion flux profiles in both positive and negative ionization modes are presented in Figure 2A and B. Through systematic analysis, XJDHT was found to contain 60 bioactive constituents, including arginine, gallic acid, quercetin, kaempferol, benzoyl paeoniflorin, stigmasterol, and sitosterol. These phytochemical components were systematically characterized based on mass spectral fragmentation patterns and database matching. The complete phytochemical profile, including retention times, molecular formulas, and mass-to-charge ratios, is comprehensively documented in Table 2.

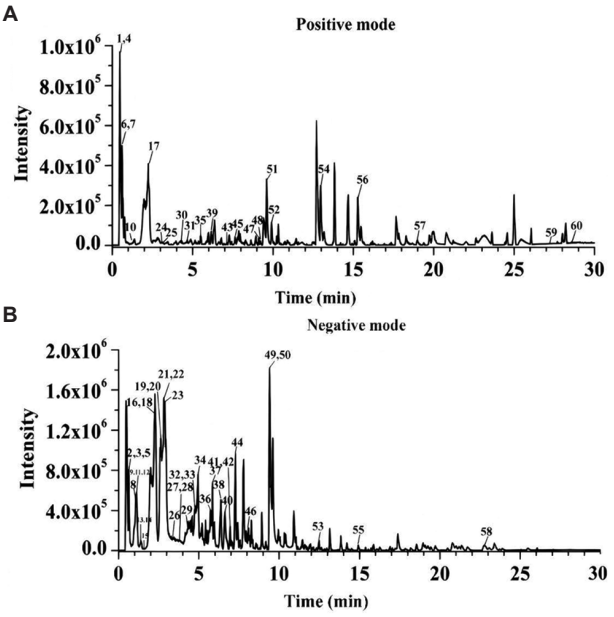

Figure 2. Basic peak ion current chromatogram of *Xijiao Dihuang* decoction in (A) positive ion mode and (B) negative ion mode

3.3. Effective component selection and sorting

In the TCMSP database, 24 components were selected, including albiflorin, paeoniflorin, berberine, and benzoyl paeoniflorin, based on the criteria of OB ≥ 30% and DL ≥ 0.18. In the SwissADME database, the conditions were

Table 2. Ingredient identification of X*ijiao Dihuang* decoction

t_R [min]	Formula	Theoretical MS	MS^1	MS/MS fragments	Identification
0.48	$C_6H_{14}N_4O_2$	175.1190	175.1188	116.0629	Arginine
0.60	$C_7H_6O_5$	169.0143	169.0144	125.0350,97.0320	Gallic acid
0.61	$C_{19}H_{26}O_{15}$	493.1199	493.1192	313.0686,169.0252,151.0049	Diglucosyl gallic acid
0.68	$C_9H_{11}NO_2$	166.0863	166.0860	120.0884,103.0616,91.0544	Phenprobamate
0.69	$C_{15}H_{24}O_9$	347.1348	347.1338	167.0716,149.0460,127.0359	Leonuride
0.71	$C_6H_6O_3$	127.0390	127.0389	109.0307,81.0352	3-hydroxy-2-methyl-4H-pyran-4-one
0.71	$C_9H_{17}NO_5$	220.1180	220.1176	184.0965,142.0858	D-pantothenic acid
0.84	$C_7H_6O_4$	153.0193	153.0191	109.04	Protocatechuic acid
1.01	$C_{23}H_{28}O_{13}S$	543.1178	543.1181	497.1585,259.0285,121.0296	Paeoniflorin sulfonate
1.16	$C_7H_6O_3$	139.0390	139.0390	121.03	Protocatechualdehyde
1.19	$C_{15}H_{14}O_6$	289.0718	289.0710	245.0819,179.0372,165.0200,151.0400,137.0249,109.0301	(+)-Catechin
1.29	$C_8H_8O_5$	183.0299	183.0296	168.0070,124.0224	Methyl gallate
1.47	$C_8H_8O_4$	167.0350	167.0345	123.05	Vanillic acid
1.5	$C_{23}H_{28}O_{11}$	525.1603	525.1629	479.2149,449.1445,327.1047,165.0558,121.0299	Albiflorin
1.67	$C_{29}H_{38}O_{16}$	687.2131	687.2131	519.1715,323.0983	Isomaltopaeoniflorin
2.20	$C_{20}H_{28}O_{12}$	459.1508	459.1500	165.06	Paeonolide
2.23	C_8H_8O	121.0648	121.0641	103.0534,91.0539	Acetophenone
2.24	$C_{16}H_{24}O_{10}$	375.1297	375.1272	345.1177,195.0671,139.0781	Debenzoyl paeoniflorin
2.61	$C_{23}H_{28}O_{11}$	525.1603	525.1609	449.1466,165.0561,121.0380	Paeoniflorin
2.67	$C_{15}H_{22}O_9$	345.1191	345.1188	183.1033,165.0917	Aucubin
2.84	$C_9H_{10}O_5$	197.0456	197.0451	169.0160,125.0256,124.0210	Ethyl gallate
2.98	$C_{15}H_{22}O_{10}$	361.1140	361.1153	199.0971,179.1052,161.0228	Monomelittin
3.02	$C_{20}H_{30}O_{12}$	461.1665	461.1627	135.04	Forsythoside E
3.19	$C_{10}H_{14}O_2$	167.1067	167.1063	149.0965,121.1033	6-pentyl-2H-pyran-2-one
3.21	$C_{10}H_{14}O$	151.1117	151.1112	133.0648,123.0798	Carvone
3.56	$C_{35}H_{46}O_{20}$	785.2510	785.2499	623.2235,161.0289	Purpureaside B
3.84	$C_{16}H_{24}O_8$	343.1398	343.1375	181.0498,151.0357	Mudanpioside F
3.86	$C_{24}H_{30}O_{15}S$	589.1233	589.1222	421.2731,258.9918	Mudanpioside E sulfite
4.17	$C_{14}H_6O_8$	300.9990	300.9987	229.02	Ellagic acid
4.42	$C_{10}H_{16}O$	153.1274	153.1269	135.1165,125.0228	Alpha-pinene oxide
4.61	$C_{27}H_{30}O_{15}$	595.1658	595.1658	287.05	Kaempferol 3-rutinoside
4.63	$C_{36}H_{48}O_{20}$	799.2666	799.2654	623.2224,175.0406	Jionoside A1
4.67	$C_{30}H_{32}O_{15}$	631.1668	631.1665	613.1577,491.1200	Galloyl paeoniflorin
5.19	$C_{23}H_{28}O_{12}$	495.1508	495.1500	165.0571,137.0616	Oxypaeoniflorin
5.41	$C_{21}H_{20}O_{12}$	465.1028	465.1009	303.1257,285.0742	Hyperoside
5.64	$C_{30}H_{32}O_{14}$	615.1719	615.1720	431.1383,281.0724,137.0323	Mudanpioside H
5.86	$C_{29}H_{36}O_{15}$	623.1981	623.1982	461.1672,161.0253	Forsythiaside
6.31	$C_{24}H_{30}O_{13}$	525.1614	525.1608	195.07	Mudanpioside E
6.32	C_9H_8O	133.0648	133.0647	115.0535,105.0694,	Trans-cinnamaldehyde
6.57	$C_{24}H_{30}O_{11}$	493.1715	493.1705	162.04	Paeonidanin
7.05	$C_{30}H_{38}O_{15}$	637.2138	637.2132	461.1699,175.0429	Jionoside D

(Cont'd...)

Table 2. *(Continued)*

tR [min]	Formula	Theoretical MS	MS^1	MS/MS fragments	Identification
7.07	$C_{37}H_{36}O_{19}$	783.1778	783.1769	465.14	3',6'-di-O-gal-loylpaeoniflorin
7.17	$C_{20}H_{17}NO_4$	336.1230	336.1231	320.0913,306.0717,292.0950,278.0809	Berberine
7.31	$C_{18}H_{24}O_{14}$	463.1093	463.1068	403.0879,373.0980,343.0660	Mudanoside B
7.62	$C_{15}H_{10}O_7$	303.0499	303.0496	257.04	Quercetin
8.04	$C_{17}H_{18}O_6$	317.1031	317.1019	121.03	Paeoniflorgenone
9.02	$C_9H_{10}O_3$	167.0703	167.0700	149.0589	Paeonol
9.15	$C_{15}H_{10}O_6$	287.0550	287.0549	165.02	Kaempferol
9.42	$C_{23}H_{26}O_{10}$	507.1497	507.1488	461.1482,431.1359,177.0558	Lactiflorin
9.43	$C_{23}H_{28}O_{11}$	525.1603	525.1602	479.1533,283.0821	Mudanpioside I
9.60	$C_{30}H_{32}O_{12}$	585.1967	585.1973	319.1251,267.0928	Benzoyl paeoniflorin
9.90	$C_9H_{10}O$	135.0804	135.0804	135.0793,107.0497	2,4-dimethylbenzaldehyde
12.47	$C_{15}H_{12}O_4$	255.0663	255.0648	227.0775,213.0549	Pinocembrin
12.96	$C_{18}H_{39}NO_3$	318.3003	318.3002	300.2897,256.2716,212.2369	Phytosphingosine
14.90	$C_{15}H_{10}O_5$	269.0456	269.0449	241.05	Apigenin
15.38	$C_{18}H_{30}O_2$	279.2319	279.2316	149.0226	β-elaeostearic acid
18.92	$C_{30}H_{46}O_4$	471.3469	471.3470	453.3325,435.3248,423.3230,407.3308,389.3201	18-β-glycyrrhetinic acid
22.8	$C_{30}H_{48}O_3$	455.3531	455.3523	-	Mairin
27.2	$C_{29}H_{50}O$	415.3934	415.3923	-	Sitosterol
28.8	$C_{29}H_{48}O$	395.3672	395.3666	257.2254,161.1316	Stigmasterol

Abbreviations: MS: Mass spectrometry; t_R: Retention time.

set to "high" GI absorption, "yes" for BBB permeability, and at least three "yes" in the five DL evaluation frameworks (Lipinski, Ghose, Veber, Egan, and Muegge), resulting in 12 components, including paeonol, carvone, phenprobamate, and pinocembrin. After deduplication of results from both databases, 24 potential active components of XJDHT were obtained: (+)-Catechin, albiflorin, paeoniflorin, ellagic acid, 2,4-dimethylbenzaldehyde, paeonol, trans-cinnamaldehyde, alpha-pinene oxide, carvone, phenprobamate, acetophenone, protocatechualdehyde, 6-pentyl-2h-pyran-2-one, 3-hydroxy-2-methyl-4h-pyran-4-one, stigmasterol, sitosterol, mairin, pinocembrin, benzoyl paeoniflorin, lactiflorin, kaempferol, paeoniflorgenone, quercetin, and berberine.

3.4. Screening of active ingredients and disease targets

The selected chemical components were input into the SwissTargetPrediction and TCMSP databases to screen for compound targets, resulting in 690 active component targets after the removal of duplicates. A search using the term "ischemic stroke" was conducted in GeneCards, OMIM, therapeutic target (Databasehttps://db.idrblab.net/ttd/), and GEO databases, restricted to the species *Homo sapiens* and including only experimentally validated genes, resulting in 3573 ischemic stroke-related disease targets. A Venn diagram was constructed to identify overlapping targets, revealing 424 intersection targets between active components and ischemic stroke, as shown in Figure 3.

3.5. Protein interaction analysis and "component–target" network construction

The STRING platform was used to obtain the protein interaction relationships. The resulting Tab-separated Values file was imported into Cytoscape3.10.2 software to generate the PPI map. Based on the degree value, the top 20 core targets were identified: Phosphatidylinositol-4,5-bisphosphate 3-kinase regulatory subunit 1 (PIK3R1), SRC proto-oncogene (SRC), signal transducer and activator of transcription (STAT) 3, phosphatidylinositol-4,5-bisphosphate 3-kinase catalytic subunit alpha (PIK3CA), phosphatidylinositol-4,5-bisphosphate 3-kinase catalytic subunit beta (PIK3CB), phosphatidylinositol-4,5-bisphosphate 3-kinase catalytic subunit delta (PIK3CD), AKT serine/threonine kinase 1 (AKT1), epidermal growth factor receptor (EGFR), mitogen-activated protein kinase (MAPK)1, heat shock protein 90 alpha class a member 1 (HSP90AA1), protein tyrosine phosphatase non-receptor

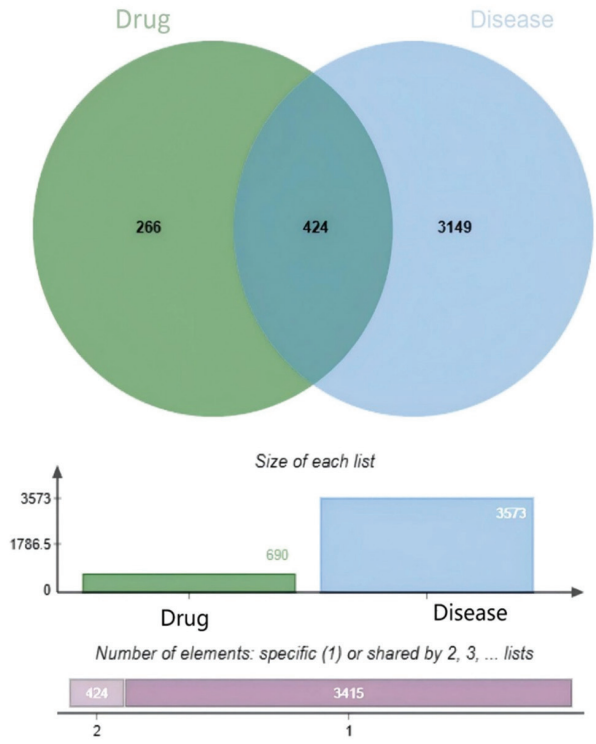

Figure 3. Intersection of effective components and ischemic stroke-related targets
Note: Green represents active drug ingredients, and blue represents the disease (ischemic stroke).

type 11, MAPK3, estrogen receptor 1 (ESR1), NRAS, Harvey rat sarcoma virus (HRAS), EP300, phospholipase C gamma 1, protein kinase A catalytic subunit alpha, MAPK8, and protein tyrosine kinase 2, as shown in Figure 4. Using the 24 active components and their associated targets, a "component–target" network diagram was constructed using Cytoscape3.10.2 software, as shown in Figure 5.

3.6. GO and KEGG enrichment analysis

The DAVID database was used to perform GO and KEGG functional enrichment analysis of the BP related to the intersection targets of active components and disease, in order to better understand the pharmacological blood-activating effect of XJDHT in the treatment of ischemic stroke. The following results were obtained, as shown in Figure 6A-C.

A total of 184 BP were associated with the 424 targets. These include phosphorylation, EGFR signaling pathway, signal transduction, insulin receptor signaling pathway, protein kinase B signaling, insulin-like growth factor receptor signaling pathway, cellular response to cadmium ion, protein phosphorylation, cellular response to reactive oxygen species (ROS), phosphatidylinositol-mediated signaling, T cell receptor signaling pathway, and T cell costimulation, among others.

Twenty-two CCs are involved in target interactions, including cytosol, plasma membrane, phosphatidylinositol 3-kinase (PI3K) complex class IA, PI3K complex, perinuclear region of differentiation, glutamatergic synapse, nucleoplasm, nucleus, and focal adhesion.

Forty-four MF were identified, including nitric oxide synthase regulator activity, protein phosphatase binding, adenosine triphosphate binding, protein kinase binding, kinase activity, phosphotyrosine binding, phosphatidylinositol-4,5-bisphosphate 3-kinase activity, 1-phosphatidylinositol-4-phosphate 3-kinase activity, protein kinase activity, and protein serine/threonine kinase activity.

KEGG pathways enrichment analysis showed that the 424 targets were involved in 147 major metabolism and signal transduction pathways, including endocrine resistance, proteoglycans in cancer, growth hormone synthesis, secretion and action, erythroblastic leukemia viral oncogene homolog (ErbB) signaling pathway, prolactin signaling pathway, EGFR tyrosine kinase inhibitor resistance, thyroid hormone signaling pathway, programmed death-ligand 1 expression and programmed cell death protein 1 checkpoint pathway in cancer, VEGF signaling pathway, and estrogen signaling pathway. These results are shown in Figure 7. The active ingredients, core targets, and core pathways are presented together in Figure 8, and the pathways with their corresponding numbers are listed in Table 3.

3.7. Selection of proteins for quantitative real-time polymerase chain reaction and expression analysis in rat brain tissue with ischemic stroke

Among the top 20 KEGG-related pathways, those with high research frequency and relatively comprehensive experimental validation included the VEGF signaling pathway, estrogen signaling pathway, lipid and atherosclerosis, and chemical carcinogenesis—receptor activation. Based on detailed KEGG pathway diagrams, signaling pathways potentially involved in ischemic stroke include the PI3K–protein kinase B (AKT) signaling pathway, MAPK signaling pathway, ErbB signaling pathway, mammalian target of rapamycin (mTOR) signaling pathway, and VEGF signaling pathway. Associated proteins include MAPK3, PIK3CA, PIK3CD, AKT1, MAPK1, HRAS, PIK3R1, PIK3CB, NRAS, SRC, EGFR, ESR1, HSP90AA1, STAT3, and EP300. After ischemic stroke model rats were treated with different reagents, the expression of related proteins in the brain tissue was detected by fluorescence qPCR to assess the

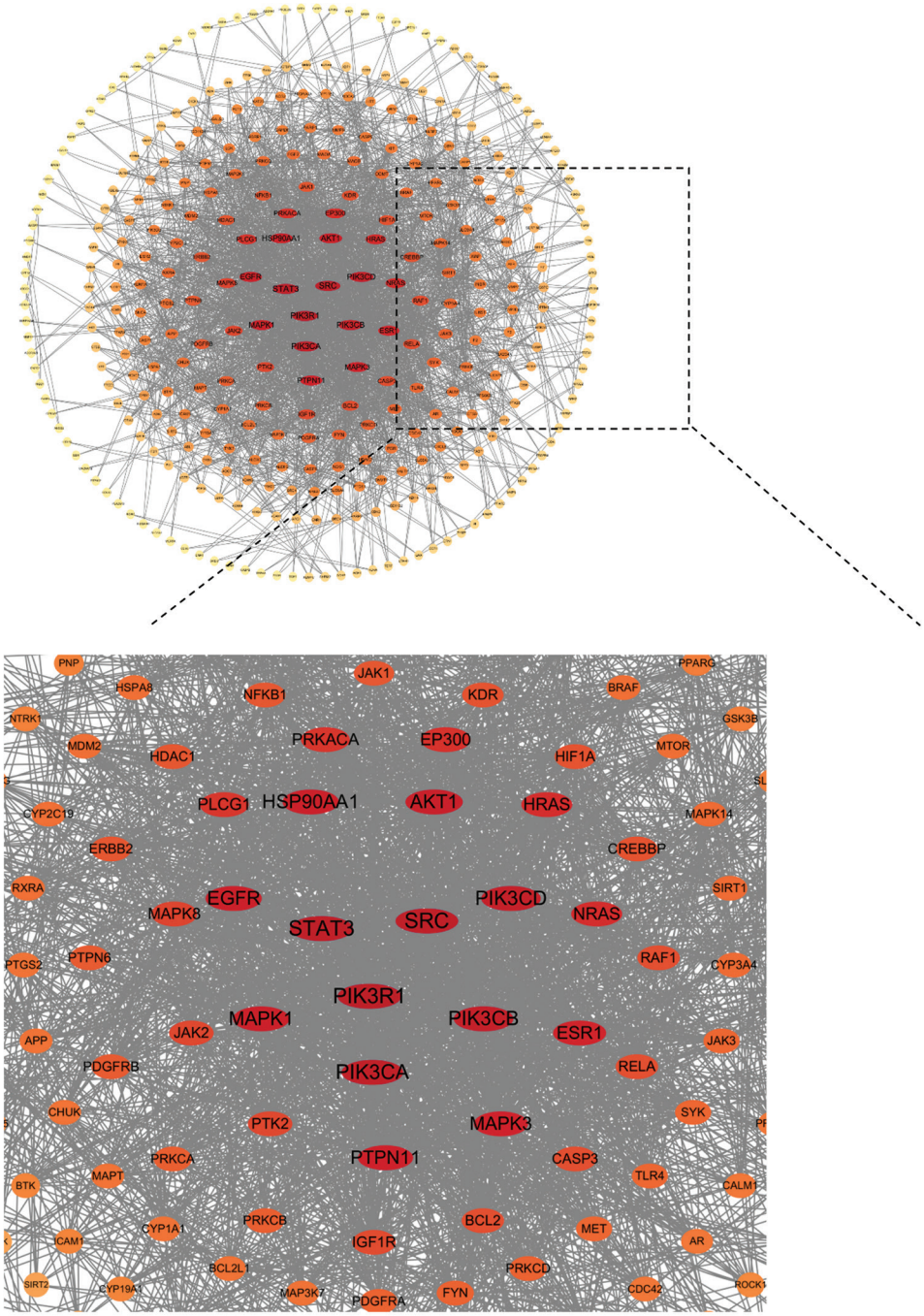

Figure 4. Protein–protein interaction network diagram
Note: Larger icons and deeper colors indicate protein with higher degree values.

therapeutic effect of XJDHT. Proteins such as MAPK3, PIK3CA, PIK3CD, AKT1, MAPK1, PIK3R1, PIK3CB, SRC, HSP90AA1, and STAT3 have been extensively studied. To explore new therapeutic mechanisms, five proteins (EP300, NRAS, EGFR, HRAS, and ESR) were selected for further investigation of their expression trends. Changes in protein levels were compared to the model group. For the HRAS protein, MCAO increased HRAS levels, while XJDHT and edaravone treatment decreased them; only the difference between the XJDHT group and the model group was statistically significant ($p<0.05$). For EGFR, MCAO and XJDHT decreased EGFR levels, whereas edaravone treatment increased EGFR levels; only the difference between the model group and

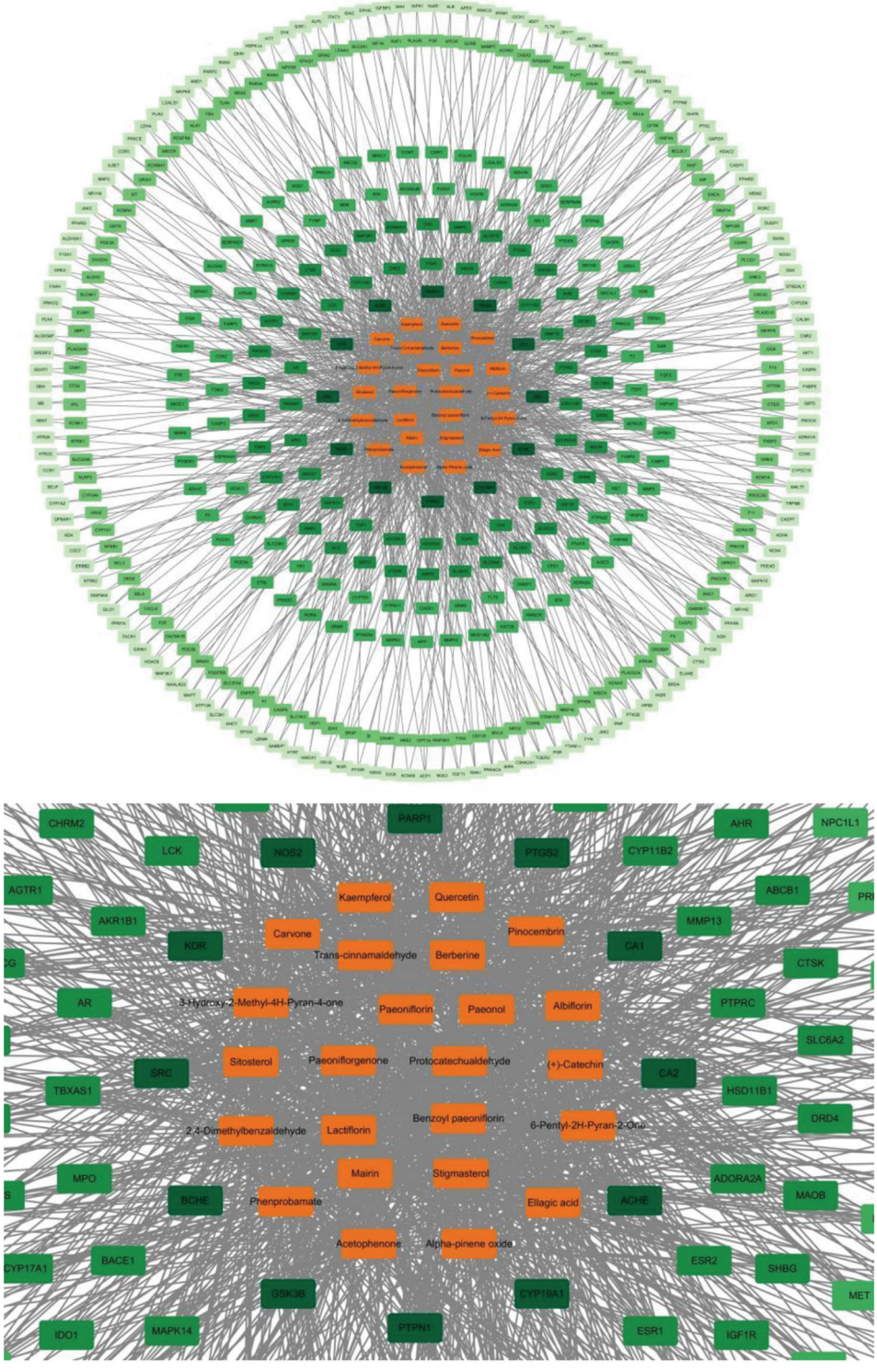

Figure 5. Component–target network diagram
Notes: Orange nodes in the center represent components, while green nodes on the periphery represent targets; Darker green indicates a higher degree value for the corresponding target.

the XJDHT group was statistically significant ($p<0.05$). For EP300, MCAO increased EP300 levels, while both treatments decreased them; the difference was statistically significant only in the XJDHT treatment group ($p<0.05$).

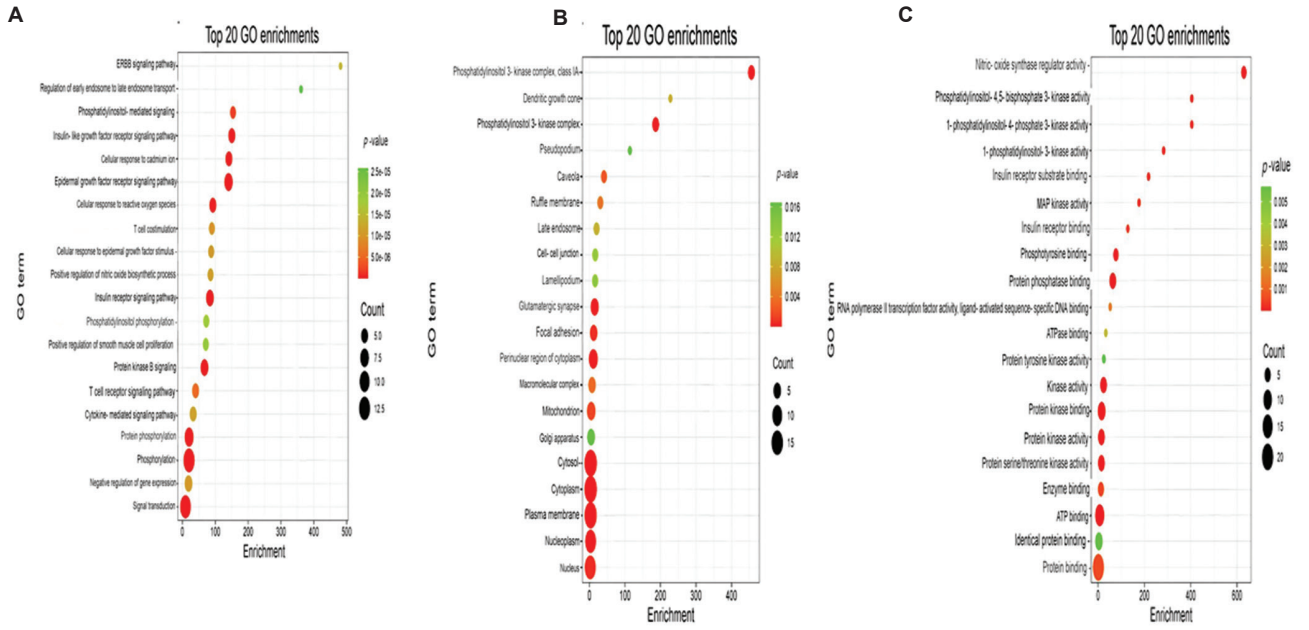

Figure 6. The top 20 Gene Ontology (GO) enrichments of (A) biological processes, (B) cellular components, and (C) molecular functions
Abbreviations: ATP: Adenosine triphosphate; ERBB: Erythroblastic Leukemia Viral Oncogene Homolog; MAP: Mitogen-activated protein kinase.

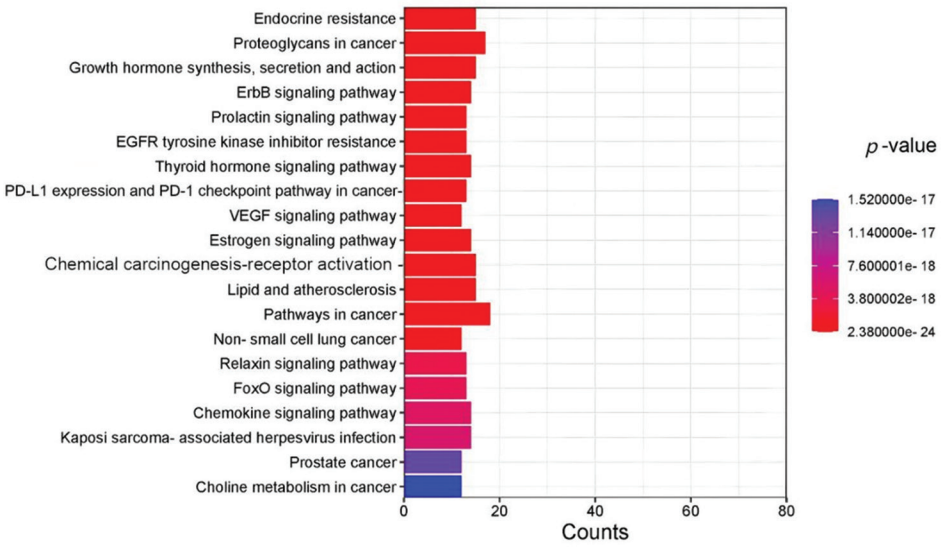

Figure 7. Top 20 Kyoto Encyclopedia of Genes and Genomes pathways
Notes: Each bar represents the number of genes associated with each pathway; A stronger correlation is indicated by a redder color.
Abbreviations: EGFR: Epidermal growth factor receptor; FoxO: Forkhead box O; PD-L1: Programmed death-ligand 1; PD-1: Programmed cell death protein 1; VEGF: Vascular endothelial growth factor.

For NRAS, MCAO increased NRAS levels, and XJDHT and edaravone decreased them, with significance only in the XJDHT treatment group ($p<0.05$). For ESR1, MCAO increased ESR1 levels, while both treatments decreased them; again, only the change in the XJDHT group was statistically significant ($p<0.05$).

Edaravone plays a neuroprotective role by scavenging free radicals and reducing oxidative stress damage to brain tissue. Studies have shown that edaravone can protect the integrity of cerebral microvessels and inhibit the overexpression of matrix metalloproteinase-9, thereby reducing vascular endothelial injury after cerebral ischemia.

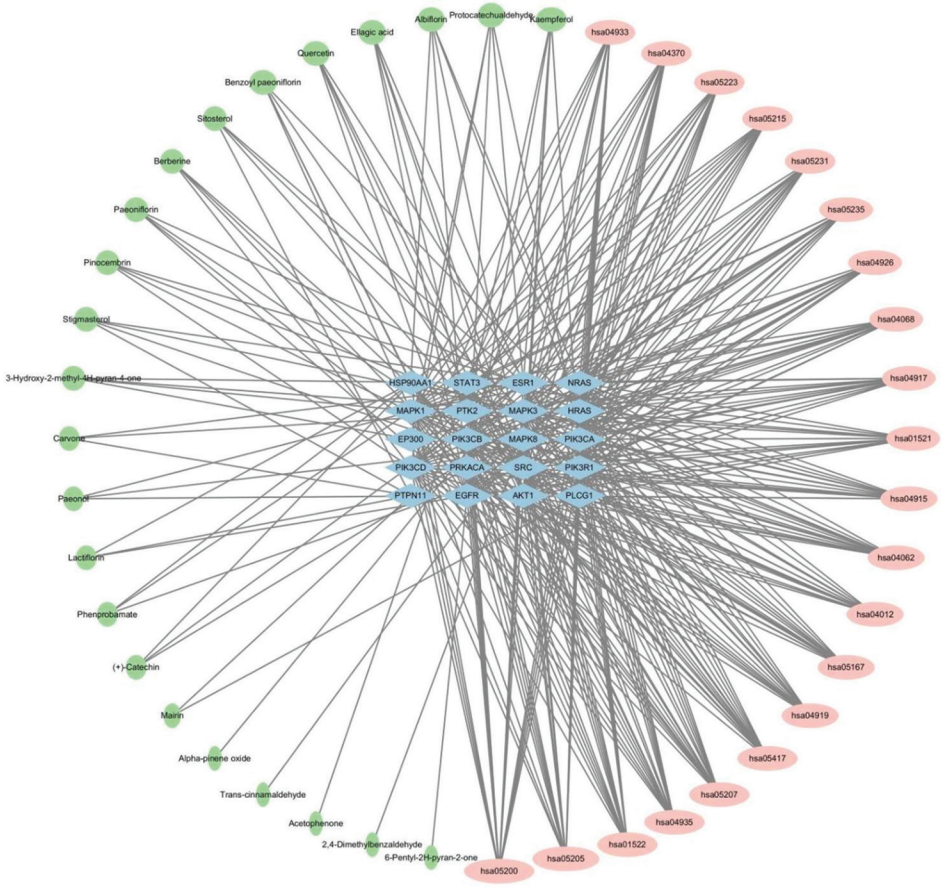

Figure 8. Relationship diagram of core components, targets, and pathways
Note: Blue represents core targets, green represents core components, and pink represents core Kyoto Encyclopedia of Genes and Genomes pathways.

In addition, edaravone delays neuronal death and improves neurological function recovery after cerebral ischemia. The related expression trends are shown in Figure 9.

3.8. Molecular docking

The qPCR results showed that changes in NRAS and EP300 proteins in the XJDHT group were more pronounced than those in the other groups. In addition, existing research is related to EP300 and NRAS; hence, the chemical components acting on these two proteins were selected for molecular docking. Molecular docking results showed that the core active compound albiflorin had a good binding affinity with NRAS, with a minimum molecular binding capacity of −8.8 kcal/mol. Hydroxy-2-methyl-4H-pyran-4-one and protocatechuic aldehyde (PCA) exhibited good binding affinity with EP300, with a minimum molecular binding capacity of −5.5 kcal/mol and −6.2 kcal/mol, respectively. Details of the optimal docking modes of hydroxy-2-methyl-4H-pyran-4-one and PCA from XJDHT with EP300 are shown in Figure 10.

3.9. Immunofluorescence staining

The immunofluorescence staining results of target proteins NRAS and EP300 in rat brain tissue showed that the average intensity of red fluorescence in the XJDHT group was lower than that in the control, model, and edaravone groups. These results indicate that the active components of XJDHT reduced the levels of NRAS and EP300 in brain tissue. The immunofluorescence staining results of the two target proteins are shown in Figure 11A and B. The EP300 level in the model group was significantly higher than in the control group, indicating that the model treatment had a significant impact on EP300 expression. The EP300 levels in the edaravone and the XJDHT groups were lower than those in the model group, indicating that the edaravone and XJDHT treatments had an inhibitory effect on the elevated EP300 expression in the model group. Similarly, the NRAS level in the model group was higher than that in the control group, with a significant difference, indicating that the model treatment increased NRAS expression. The NRAS levels in the edaravone and XJDHT groups

Table 3. Core KEGG pathways and their corresponding abbreviations

Abbreviation	Core KEGG pathway
hsa05200	Pathways in cancer
hsa05417	Lipid and atherosclerosis
hsa01521	EGFR tyrosine kinase inhibitor resistance
hsa04933	AGE-RAGE signaling pathway in diabetic complications
hsa04066	HIF-1 signaling pathway
hsa05205	Proteoglycans in cancer
hsa04080	Neuroactive ligand-receptor interaction
hsa05215	Prostate cancer
hsa04020	Calcium signaling pathway
hsa04014	Ras signaling pathway
hsa05167	Kaposi sarcoma-associated herpesvirus infection
hsa05161	Hepatitis B
hsa04024	cAMP signaling pathway
hsa05230	Central carbon metabolism in cancer
hsa04370	VEGF signaling pathway
hsa04151	PI3K–AKT signaling pathway
hsa05207	Chemical carcinogenesis–receptor activation
hsa05235	PD-L1 expression and PD-1 checkpoint pathway in cancer
hsa05212	Pancreatic cancer
hsa01522	Endocrine resistance

Abbreviations: AGE: Advanced glycation end-products; AKT: Protein kinase B; cAMP: Cyclic adenosine monophosphate; EGFR: Epidermal growth factor receptor; HIF-1: Hypoxia-inducible factor 1; PD-L1: Programmed death-ligand 1; PD-1: Programmed cell death protein 1; PI3K: Phosphatidylinositol 3-kinase; RAGE: Receptor for advanced glycation end-products; VEGF: Vascular endothelial growth factor; KEGG: Kyoto Encyclopedia of Genes and Genomes.

were lower than those in the model group, suggesting that edaravone and XJDHT treatments might inhibit the elevated NRAS expression in the model group.

4. Discussion

China has experienced an 86.0% increase in ischemic stroke incidence since 1990, currently accounting for 3.94 million new cases annually.[7] Researchers have demonstrated that XJDHT can significantly improve neurological function in patients[8] or mice suffering from ischemic stroke in both clinical trials and basic experiments.[9] The therapeutic efficacy rate of XJDHT in stroke patients has been shown to reach 98.0%, according to comprehensive clinical evaluations.[8] Through the integration of network pharmacology approaches with systematic experimental validation, this study elucidates the therapeutic efficacy and underlying molecular mechanisms of XJDHT in the treatment of ischemic stroke.

This study identified 24 active ingredients and 690 therapeutic targets associated with XJDHT, along with 3573 ischemic stroke-related targets retrieved from public databases. Through cross-analysis, 424 overlapping targets were identified between XJDHT components and ischemic stroke pathology. Network pharmacological analysis revealed 10 core bioactive compounds: Ellagic acid, kaempferol, pinocembrin, sitosterol, stigmasterol, PCA, carvone, albiflorin, paeoniflorin, and benzoyl paeoniflorin.

The qPCR validation results prompted further investigation into EP300 and NRAS targets, along with their corresponding active constituents: Hydroxy-2-methyl-4H-pyran-4-one, PCA, and albiflorin, for subsequent mechanistic exploration.

EP300, also known as histone acetyltransferase p300, is a nuclear enzyme encoded by the *EP300* gene.[10] EP300 overexpression is associated with prostate cancer, breast cancer, hepatocellular carcinoma, and non-small cell lung cancer and is therefore considered a potential therapeutic target in oncology.[11] It regulates gene expression through the acetylation of histones and other transcription factors, thereby affecting chromatin structure and function and contributing to fibrosis development, making it a potential target for anti-fibrosis therapies.[12] In neurological diseases, EP300 is recruited to specific gene enhancer regions by interacting with the transcription factor TFAP2β in the core transcriptional regulatory circuit of neuroblastoma, thereby regulating the expression of genes associated with the malignant phenotype of neuroblastoma cells.[13] A carboxypeptidase vitelloin-like protein promotes glioma progression by inhibiting the signal STAT 1 pathway through interaction with the Bruton's tyrosine kinase/p300 axis.[14]

Accumulating evidence from recent investigations indicates that EP300 serves as a pivotal regulator in cellular survival mechanisms, particularly through transcriptional modulation of apoptosis-related genes and chromatin remodeling processes.[13] Its association with stroke pathogenesis is manifested through regulatory effects on inflammatory responses and autophagy mechanisms. Under ischemic conditions, mTORC1 inhibition induces unc-51-like autophagy activating kinase 1 phosphorylation, thereby enhancing autophagic flux. This activated autophagy pathway facilitates the degradation of impaired cellular constituents during cerebral ischemia, demonstrating a critical neuroprotective mechanism.[15] EP300 can acetylate the raptor protein in the mTORC1 complex; acetylation of the raptor facilitates the binding of mTORC1 to lysosomes, thereby promoting its activity and inhibiting autophagy.[16] Furthermore, EP300 exerts inhibitory effects on autophagy initiation by mediating the acetylation of the PI3K catalytic

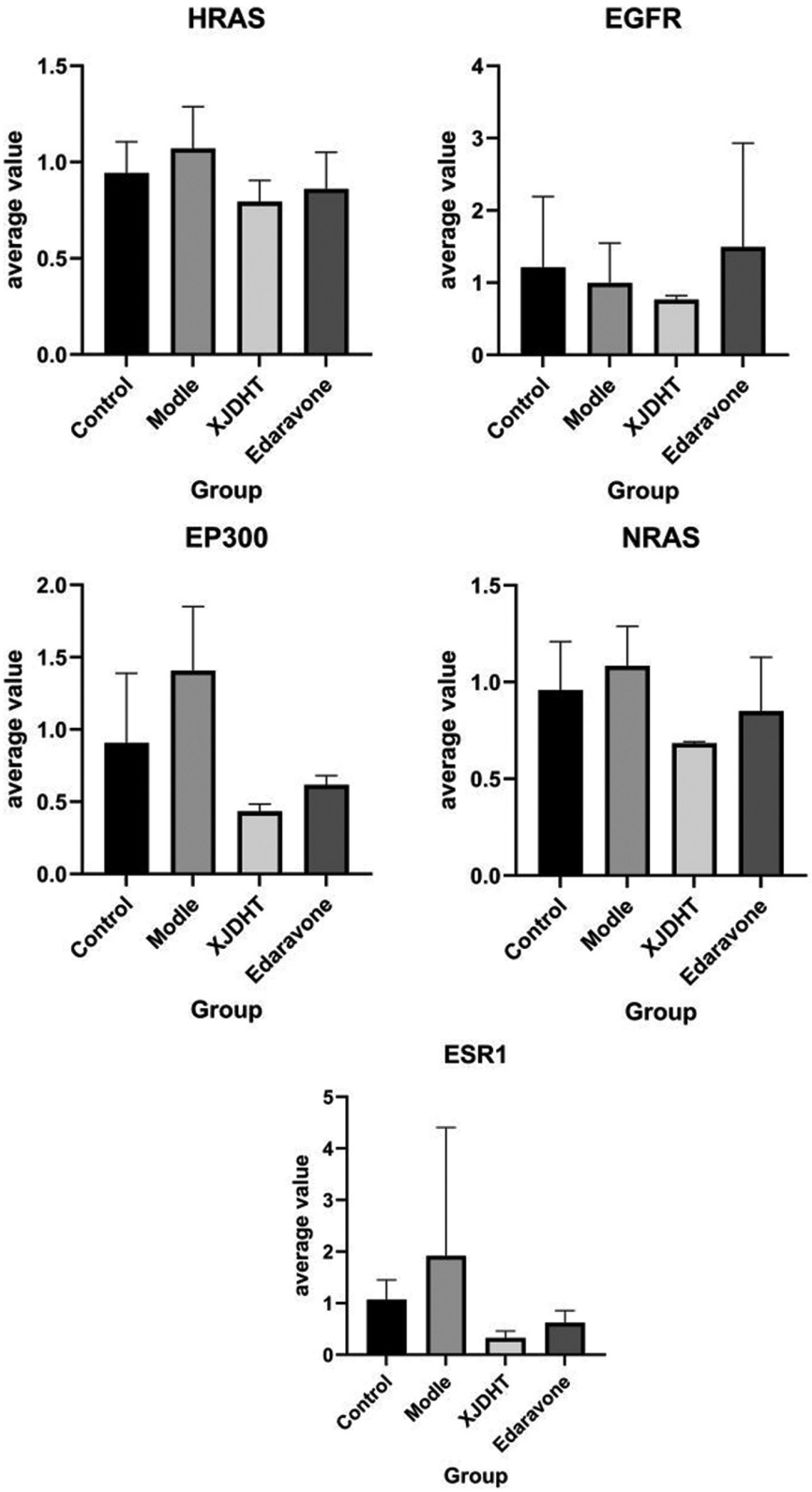

Figure 9. Expression trends of *binding protein P300*, *NRAS*, *EGFR*, *HRAS*, and *ESR1* detected with quantitative polymerase chain reaction
Abbreviations: EGFR: Epidermal growth factor receptor; ESR1: Estrogen receptor 1; HRAS: Harvey rat sarcoma virus; NRAS: Neuroblastoma RAS viral oncogene homolog.

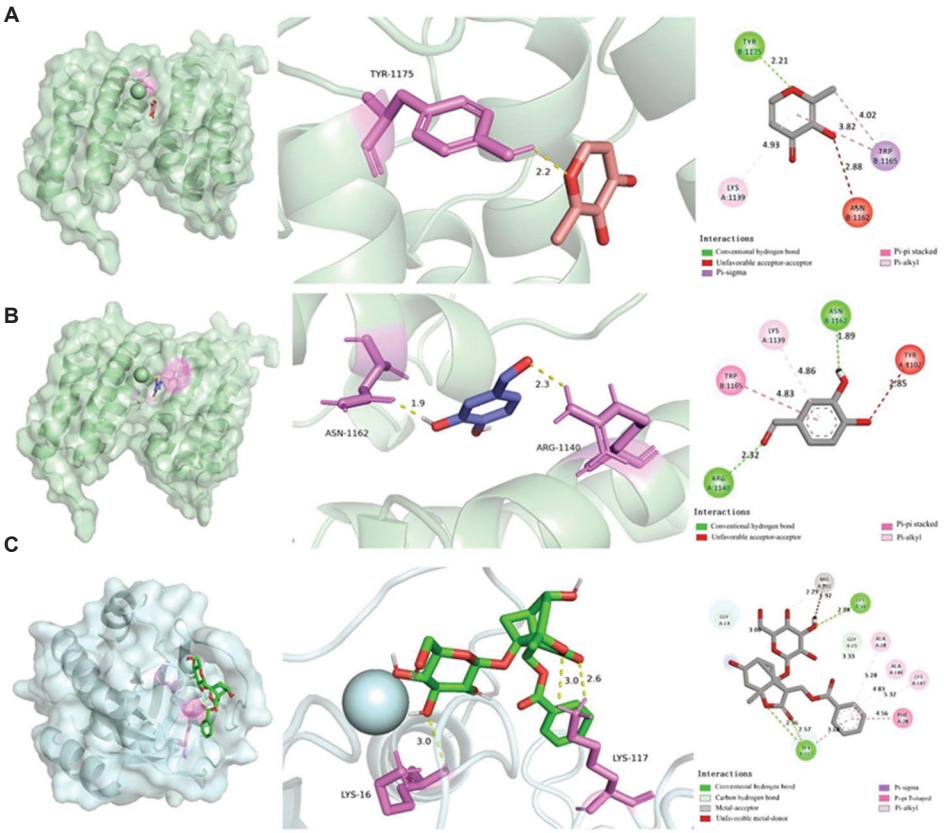

Figure 10. Molecular docking of hydroxy-2-methyl-4H-pyran-4-one and protocatechuic aldehyde from *Xijiao Dihuang* decoction with binding protein P300 (EP300). (A) Schematic representation of EP300 binding to hydroxy-2-methyl-4H-pyran-4-one. (B) Schematic representation of EP300 binding to protocatechuic aldehyde. (C) Schematic representation of the neuroblastoma RAS viral oncogene homolog binding to albiflorin.
Abbreviations: ALA: Alanine; ARG: Arginine; ASN: Asparagine; GLY: Glycine; MG: Magnesium ion; PHE: Phenylalanine; LYS: Lysine; TYR: Tyrosine; TRP: Tryptophan.

subunit type 3 (PIK3C3/VPS34) complex.[17] PIK3C3 affects the process of neuroinflammation by regulating autophagy in microglia.[18] During ischemic injury in neuronal cells, the autophagic pathway is initiated through activation of microtubule-associated protein 1 light chain 3. This critical autophagy marker undergoes proteolytic cleavage and lipidation to form the LC3-II isoform, which subsequently anchors to autophagosomal membranes through covalent conjugation. This molecular transformation facilitates autophagosome biogenesis and maturation during cellular stress responses.[19] EP300 inhibits autophagosome biogenesis by suppressing the LC3 lipidation process.[20] Following ischemic stroke, syntaxin 17 (STX17) facilitates cellular clearance of damaged organelles and misfolded proteins by mediating autophagosome–lysosome fusion, thereby mitigating ischemia-induced neuronal damage via enhanced autophagic flux.[21] EP300 impairs autophagosome–lysosome fusion through acetylation-mediated modulation of STX17.[22] Experimental evidence demonstrates that both aspirin and its bioactive metabolite salicylate elicit autophagic responses through selective inhibition of EP300 acetyltransferase activity.[23]

In addition, EP300 promotes the development of inflammation through transcriptional regulation by controlling the expression of cytokines and chemokines and activating the function of inflammatory cells. The increased expression of p53 protein in ischemic regions promotes neuronal apoptosis.[24] Acetylation of p53 by EP300 enhances its transcriptional activity and protects it from degradation.[25] During the pathogenesis of ischemic stroke, tumor necrosis factor (TNF)-α initiates a cascade of inflammatory responses by stimulating the synthesis and release of secondary inflammatory mediators. This cytokine-mediated process facilitates the recruitment and subsequent activation of immunocompetent cells within the neurovascular unit, thereby exacerbating secondary neuronal injury through amplified inflammatory mechanisms.[26] In addition, TNF-α can lead to the destruction of the BBB and increase the permeability of brain tissue, allowing more inflammatory cells and substances to enter the brain and aggravate the

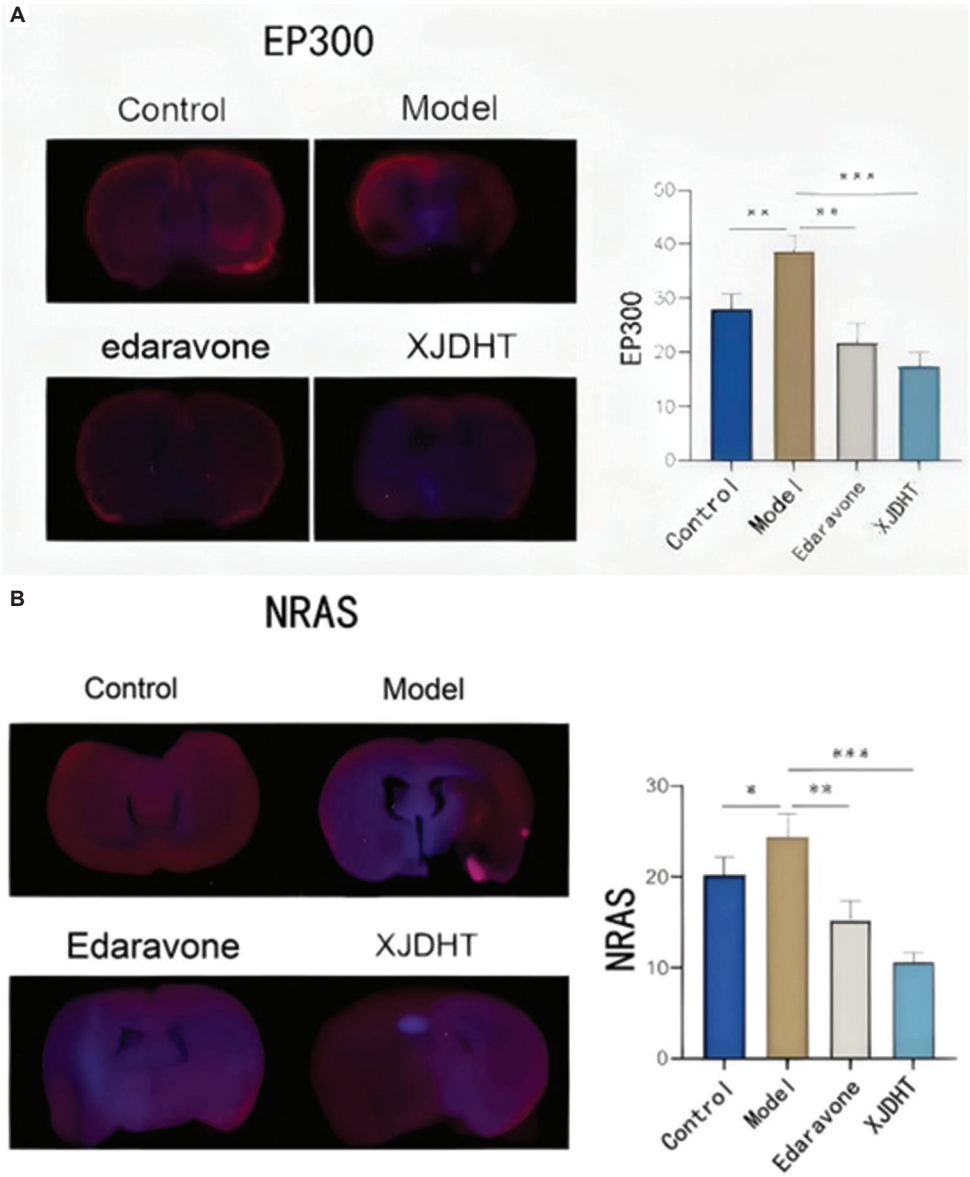

Figure 11. Immunofluorescence staining of NRAS and binding protein P300 (EP300) in brain tissue. (A) Distribution and intensity of EP300 staining in brain tissue sections from each group. (B) Distribution and intensity of NRAS staining in brain tissue sections from each group.
Notes: *p<0.05; **p<0.01; ***p<0.001
Abbreviations: NRAS: Neuroblastoma RAS viral oncogene homolog; XJDHT: *Xijiao Dihuang* decoction.

injury.[27] EP300 potentiates the transcriptional activity of TNF-α both through direct interactions with promoter-bound transcription factors and via dual mechanisms involving chromatin remodeling[12] or regulation of the NF-κB signaling pathway.[28]

Hydroxy-2-methyl-4H-pyran-4-one (commonly termed maltol), an EP300-modulating compound, demonstrates significant neuroprotective effects in stroke intervention. Experimental evidence reveals that maltol administration exerts dual antioxidant mechanisms: Not only does it attenuate oxidative stress through marked reductions in ROS generation and malondialdehyde accumulation in cerebral tissues, but it also enhances antioxidant enzyme activity. Mechanistic studies further indicate that maltol-mediated neuroprotection involves potentiation of the PI3K/AKT/nuclear factor erythroid 2-related factor 2 (NRF2) signaling axis, as evidenced by increased phosphorylation levels of PI3K, AKT, and NRF2.[29] Regarding its anti-inflammatory properties, maltol has been shown to significantly inhibit the production of pro-inflammatory mediators through downregulation

of the PI3K/AKT/NF-κB signaling pathway.[30] Maltol suppresses the phosphorylation of p38 proteins, effectively blocking activation of the p38 MAPK signaling pathway and consequently mitigating cellular inflammatory responses.[31]

Comprehensive analysis of the forkhead box O signaling pathway mapping via the KEGG database revealed that both PI3K–AKT and MAPK signaling pathways occupy upstream regulatory positions relative to EP300. The PI3K/AKT signaling axis modulates EP300 activity through targeted phosphorylation mechanisms. Specifically, AKT-mediated phosphorylation modifies the binding dynamics between EP300 and associated transcription factors, consequently inducing transcriptional regulation of downstream genes.[32] Following activation of the Janus kinase–STAT signaling cascade, STAT transcription factors undergo nuclear translocation and form functional complexes with the EP300 transcriptional coactivator, thereby orchestrating the transcriptional activation of cognate target genes.[33] The MAPK signaling pathway catalyzes the phosphorylation of EP300 through kinase activation. This post-translational modification potentiates the transcriptional coactivator function of EP300, thereby inducing transcriptional activation of downstream target genes.[34]

These findings suggest that maltol may exert therapeutic effects against ischemic stroke through a mechanism involving the inhibition of EP300 phosphorylation via dual modulation of the PI3K/AKT and MAPK signaling pathways. This regulatory action consequently reduces EP300 acetylation levels, thereby suppressing downstream autophagic processes while simultaneously modulating pro-inflammatory responses.

Maltol has been demonstrated to suppress NOD-like receptor protein 3 (NLRP3) inflammasome activation and attenuate the release of pro-inflammatory cytokines interleukin (IL)-1β and IL-18, a phenomenon mediated through its inhibitory effects on ROS generation and caspase-1 enzymatic activity.[35] Maltol promotes nuclear accumulation of transcription factor EB via 5'-adenosine monophosphate-activated protein kinase/mTOR pathway activation to enhance lysosomal function and attenuate autophagy-dependent apoptosis.[36] Nevertheless, the potential existence of a direct regulatory relationship between EP300 and the AMPK/MTOR signaling pathway warrants additional investigation.

Another pharmacologically active compound exerting inhibitory effects on EP300 has been identified as PCA, a primary water-soluble constituent derived from *Salvia miltiorrhiza* Bunge (Lamiaceae), which has been extensively utilized in TCM for cardiovascular therapeutics.[37] Its therapeutic intervention in stroke manifests through multifaceted mechanisms, including autophagy enhancement, anti-inflammatory activity, antioxidant effects, neural regeneration promotion, and apoptosis inhibition. Mechanistically, PCA induces mitophagy activation via the NRF2/PTEN-induced kinase 1/Parkin signaling pathway. Furthermore, experimental evidence demonstrates its capacity to upregulate autophagy-related proteins through modulation of silent information regulator 1 (SIRT1), thereby establishing a dual-pathway regulatory mechanism in autophagic processes.[38] SIRT1 inhibits the transcriptional activation of EP300 by deacetylating EP300 and reducing its acetyltransferase activity.[39] A study showed that MCAO and oxygen-glucose deprivation increased the expression of NLRP3, IL-1β, and NIMA-associated kinase 7, which could be reversed by treatment with PCA.[40] The post-translational acetylation of the EP300 transcriptional coactivator potentiates NLRP3 inflammasome complex assembly and stimulates the secretion of pro-inflammatory cytokines, including IL-1β and IL-18.[41] IL-1β activates the NF-κB and MAPK signaling pathways through its receptor, and activation of these pathways, in turn, promotes EP300 expression and activity.[42] Microglia are immune cells in the central nervous system that are activated during the inflammatory response in stroke. PCA can inhibit inflammation by regulating the polarization state of microglia.[43] EP300 affects the expression of inflammation-related genes and forms immune memory by regulating H3K27ac deposition in microglia. The EP300 inhibitor GNE-049 can inhibit the formation of epigenetic memory and reduce the inflammatory response. It is speculated that PCA may also be a potential EP300 inhibitor.

In TNFα-induced endothelial injury model, PCA inhibits the migration and proliferation of vascular smooth muscle cells and prevents vascular stenosis by inhibiting the NF-κB signaling pathway and reducing the expression of hypoxia-inducible factor 1-alpha (HIF-1α). Meanwhile, TNF-α and other cytokines can mediate the expression of EP300 through NF-κB.[44] Some scholars have confirmed that PCA can improve mitochondrial energy metabolism in the internal capsule after cerebral ischemia/reperfusion, and this mechanism is associated with the inhibition of HIF1α/pyruvate dehydrogenase kinase 1 signaling pathway.[45] Therefore, PCA may inhibit EP300 expression through the NF-κB signaling pathway, thereby reducing HIF-1α acetylation and inhibiting HIF-1α function in the stroke model.

The neuroprotective mechanisms of maltol and PCA in cerebral ischemia appear to involve multiple pathways: (i) Inhibition of EP300-mediated transcriptional regulation;

(ii) activation of autophagic clearance pathways through lysosomal degradation mechanisms; (iii) suppression of aberrant vascular endothelial cell proliferation that predisposes to neovascular stenosis; and (iv) mitigation of neuroinflammatory injury through cytokine modulation in cerebral parenchyma.

Neuroblastoma RAS viral oncogene homolog, a member of the RAS gene family, plays an important role in cell signaling.[46] NRAS mutations are common in melanoma.[47] These mutations are closely related to the occurrence of bone marrow sympathetic neuropathy in hematopoietic system malignancies. Studies have found that NRAS mutations may cause myeloid proliferation and matrix damage by affecting neural signaling in the bone marrow microenvironment, thereby triggering neuropathy.[48]

NRAS gene mutations are also associated with some nervous system diseases, such as neuroblastoma and neurofibromatosis. At present, there is no direct and clear association between NRAS and stroke. However, the N-Ras protein encoded by the *NRAS* gene is part of the RAS/MAPK signaling pathway, which is involved in cell growth, division (proliferation), and differentiation.[49] In the pathogenesis of ischemic stroke, activation of the RAS/MAPK signaling pathway initiates critical pathophysiological cascades. Contemporary research elucidates that p38 MAPK signaling pathway activation demonstrates a significant correlation with neuronal apoptosis in cerebral ischemia-reperfusion injury. Activation of p38 MAPK facilitates neuronal apoptosis; conversely, pharmacological inhibition of this pathway demonstrates neuroprotective potential by attenuating post-stroke neurological deficits. Mechanistic studies reveal that p38 MAPK modulates apoptosis through phosphorylation-dependent regulation of downstream transcription factors and pro-apoptotic protein activation.[50] Emerging evidence indicates that the p38 MAPK signaling pathway mediates cerebral ischemic tolerance induced by cerebral ischemic pre-conditioning through coordinated interactions with downstream regulatory molecules, including peroxisome proliferator-activated receptor γ and NF-κB.[51]

Neuroblastoma RAS viral oncogene homolog promotes cell cycle progression by activating the MAPK signaling pathway. Activation of the MAPK pathway activates extracellular signal-regulated kinase (ERK) 1/2 and p38 MAPK pathways, which promote the activation of microglia (the major immune cells in the brain) and polarize them into proinflammatory M1 type. M1 microglia release a large number of proinflammatory cytokines (such as TNF-α, IL-1β, and IL-6), which aggravate the inflammatory response in brain tissue.[52] The ERK signaling pathway potentiates the production of ROS through the activation of nicotinamide adenine dinucleotide phosphate oxidase and associated signaling cascades, thereby exacerbating the inflammatory cascade via oxidative stress mechanisms.[53] NRAS interacts with PI3K and promotes its activation. Activated PI3K generates phosphatidylinositol triphosphate, which further activates AKT. AKT activation promotes mTOR signaling pathway activation and inhibits autophagy.[54] The constitutive activation of the PI3K–AKT signaling pathway has been implicated in maintaining microglial hyperactivity, driving excessive generation of ROS and proinflammatory cytokines, which collectively potentiate neuroinflammatory pathogenesis through sustained neuroimmune dysregulation.[55]

Albiflorin is a monoterpene glycoside extracted from the roots of the Ranunculaceae plant *Paeonia lactiflora* Pall. Albiflorin significantly improves cell survival rate, reduces intracellular ROS levels, restores mitochondrial transmembrane potential, increases the expression of anti-apoptotic proteins Bcl-2 and Bcl-X, inhibits the expression of the apoptosis marker protein Cleaved Caspase 3, and increases the phosphorylation level of AKT/glycogen synthase kinase 3 beta (GSK-3β).[56] Upon activation, AKT phosphorylates GSK-3β at the Ser9 residue, a post-translational modification that induces conformational alterations in GSK-3β, resulting in its functional inactivation through steric hindrance of the substrate-binding domain.[57] GSK-3β modulates NRAS protein stability through the regulation of leucine zipper-like transcription regulator 1 (LZTR1) activity, a substrate-specific adaptor for the E3 ubiquitin ligase complex that targets Ras family proteins for proteasomal degradation. Mechanistically, LZTR1 facilitates the recruitment of NRAS and other Ras-related proteins to the ubiquitin-proteasome system, thereby controlling their cellular abundance through targeted protein degradation. GSK-3β functions as a negative regulator of the LZTR1–Ras protein interaction. Experimental results demonstrated that pharmacological inhibition of GSK-3β significantly enhanced the binding affinity between LZTR1 and Ras proteins.[58] LZTR1-mediated proteasomal degradation of NRAS was significantly potentiated.

Albiflorin exerts inhibitory effects on oxidative and inflammatory damage *in vivo* through mechanisms involving the suppression of p38 MAPK phosphorylation. This inhibition subsequently attenuates inflammatory responses by mitigating the secretion of pro-inflammatory cytokines and modulating associated signaling pathways.[59] Albiflorin demonstrates the capacity to significantly attenuate malondialdehyde levels while concurrently enhancing superoxide dismutase

enzymatic activity. This phytochemical compound effectively suppresses ROS generation, thereby conferring cytoprotective effects against oxidative stress-induced cellular damage through comprehensive modulation of redox homeostasis.[60] Conversely, albiflorin exerts inhibitory effects on neuroinflammatory responses in post-stroke rat models through modulation of the phosphoglycerate kinase 1 (PGK1)/NRF2/heme oxygenase 1 signaling axis. Mechanistically, albiflorin facilitates PGK1 degradation while inducing sequential activation of the NRF2 signaling cascade, thereby mediating dual therapeutic effects encompassing anti-inflammatory activity and attenuation of oxidative stress-induced pathological progression.[61] NRF2 activation leads to increased expression of antioxidant enzymes that can rapidly remove ROS and prevent further cell damage.[62] The expression of NRF2 downstream genes, such as antioxidant enzymes, alleviates oxidative stress and thus acts as a buffer against excessive activation of the MAPK pathway. This process helps to maintain intracellular redox balance.[63] The suppression of ROS levels induces a significant decrease in oxidative post-translational modulation of NRAS proteins, thereby attenuating their guanosine triphosphate-binding capacity and subsequent enzymatic activity. This biochemical alteration subsequently leads to the inhibition of critical downstream signaling cascades, particularly the MAPK/ERK signaling cascade.[64]

Although limited empirical evidence exists regarding the direct pharmacological effects of albiflorin on NRAS, this compound demonstrates regulatory potential through downstream mediators of the NRAS signaling pathway to mitigate inflammatory and oxidative processes. Notably, albiflorin mechanistically modulates lysine-specific demethylase 1 (LSD1)-mediated microglial activation and ferroptosis pathways, thereby ameliorating neuroinflammatory responses in experimental models.[65] Albiflorin ameliorates cerebral ischemic injury via dual modulation of ferroptosis inhibition and autophagy activation through the PI3K/AKT signaling pathway in MCAO models.[66] Albiflorin exerts inhibitory effects on the c-Jun N-terminal kinase (JNK) signaling pathway, resulting in attenuation of astrocyte activation and pro-inflammatory chemokine secretion.[67] The potential regulatory effects of LSD1 enzymatic activity, the PI3K/AKT signaling pathway, JNK phosphorylation status, and related biochemical mediators on NRAS protein expression levels and post-translational activation mechanisms warrant comprehensive investigation through systematic experimental validation.

In this investigation, NRAS was selected as the molecular target of albiflorin for mechanistic exploration. Our findings suggest that XJDHT's therapeutic efficacy in stroke may be mediated through albiflorin's regulation of the AKT/GSK-3β signaling pathway. Specifically, Albiflorin demonstrates significant inhibitory effects on GSK-3β enzyme activity, thereby reducing NRAS biosynthesis. Furthermore, the compound effectively modulates NRAS–guanosine triphosphate binding dynamics and enzymatic function through ROS level modulation.

5. Conclusion

This study represents the first comprehensive application of multinetwork modeling to investigate the pharmacological mechanism of XJDHT in ischemic stroke treatment, providing novel insights into its therapeutic potential. Systematic network pharmacology analysis identified 24 bioactive components and 424 compound-associated targets relevant to ischemic stroke pathology. Among these, 12 principal active compounds were characterized, including kaempferol, albiflorin, ellagic acid, quercetin, benzoyl paeoniflorin, PCA, paeoniflorin, berberine, pinocembrin, sitosterol, stigmasterol, and 3-hydroxy-2-methyl-4H-pyran-4-one, all of which have been experimentally validated for diverse pharmacological activities. Pathway enrichment analysis revealed that XJDHT's neuroprotective effects are potentially mediated through modulation of MAPK, PI3K–AKT, mTOR, ErbB, and VEGF signaling pathways. Building upon prior research, molecular docking studies identified EP300 and NRAS as critical target proteins, demonstrating that maltol and PCA in XJDHT exert therapeutic effects against ischemic stroke by enhancing autophagy and suppressing inflammatory responses. Furthermore, albiflorin was shown to alleviate neuronal damage through dual mechanisms of anti-inflammatory action and oxidative stress reduction.

These findings elucidate the molecular mechanism underlying XJDHT and establish a theoretical framework for its clinical implementation. However, the current constraints in TCM phytochemical databases necessitate cautious interpretation of network pharmacology predictions, and the incomplete experimental validation of identified targets warrants further investigation. Subsequent research should prioritize comprehensive *in vivo* efficacy assessments of XJDHT in ischemic stroke models, coupled with mechanistic studies to validate the predicted signaling pathways and molecular interactions.

Acknowledgments

We wish to thank Dr. Qiuchi Zhang and Prof. Yuan Zhou for their guidance and support in the preparation of this manuscript.

Funding

This research was partially supported by the Key Project of Medical Research of the Jiangsu Commission of Health (K2023009) and the Natural Science Foundation of Nanjing University of Chinese Medicine (XZR2023030). The financial support was used to cover experimental expenses.

Conflict of interest

Zhaoyao Chen is the Youth Editorial Board Member of this journal but was not involved in the editorial and peer-review process conducted for this paper, either directly or indirectly. Separately, other authors declare that they have no known competing financial interests or personal relationships that could have influenced the work reported in this paper.

Author contributions

Conceptualization: Zhaoyao Chen
Data curation: Qiuhua He, Yujie Wang
Funding acquisition: Zhaoyao Chen
Investigation: Fantao Song
Methodology: Qiuhua He
Visualization: Qiuhua He
Writing – original draft: Qiuhua He
Writing – review & editing: Zhaoyao Chen

Ethic approval and consent to participate

All animal experiments were conducted in accordance with the guidelines of the Animal Ethics Committee in the Affiliated Hospital of Nanjing University of Traditional Chinese Medicine. Ethical approval was obtained from the Laboratory Animal Ethics Committee, [Hospital of Nanjing University of Traditional Chinese Medicine] (Approval Number: 2023DW-085-01). All procedures followed the "3R principle" (Replacement, Reduction, Refinement).

Consent for publication

Not applicable.

Availability of data

All data supporting the findings of this study are available from the corresponding author upon reasonable request and without restriction.

References

1. Zhang S, Zhang X, Wang X, *et al*. Maltol inhibits oxygen glucose deprivation-induced chromatinolysis in SH-SY5Y cells by maintaining pyruvate level. *Mol Med Rep*. 2023;27(3):75.

   doi: 10.3892/mmr.2023.12962

2. Xiong Y, Wakhloo AK, Fisher M. Advances in acute ischemic stroke therapy. *Circ Res*. 2022;130(8):1230-1251.

   doi: 10.1161/CIRCRESAHA.121.319948

3. Bu L, Dai O, Zhou F, *et al*. Traditional chinese medicine formulas, extracts, and compounds promote angiogenesis. *Biomed Pharmacother*. 2020;132:110855.

   doi: 10.1016/j.biopha.2020.110855

4. Fei X, Zhang X, Wang Q, *et al*. Xijiao dihuang decoction alleviates ischemic brain injury in MCAO rats by regulating inflammation, neurogenesis, and angiogenesis. *Evid Based Complement Alternat Med*. 2018;2018:5945128.

   doi: 10.1155/2018/5945128

5. Zhang X, Fei X, Tao W, *et al*. Neuroprotective effect of modified xijiao dihuang decoction against oxygen-glucose deprivation and reoxygenation-induced injury in PC_{12} Cells: Involvement of TLR_4-MyD88/NF- κB signaling pathway. *Evid Based Complement Alternat Med*. 2017;2017:3848595.

   doi: 10.1155/2017/3848595

6. Zhao L, Zhang H, Li N, *et al*. Network pharmacology, a promising approach to reveal the pharmacology mechanism of Chinese medicine formula. *J Ethnopharmacol*. 2023;309:116306.

   doi: 10.1016/j.jep.2023.116306

7. Ma Q, Li R, Wang L, *et al*. Temporal trend and attributable risk factors of stroke burden in China, 1990-2019: An analysis for the global burden of disease study 2019. *Lancet Public Health*. 2021;6(12):e897-e906.

   doi: 10.1016/S2468-2667(21)00228-0

8. Jing J, Jing-Bo L, Ming-Ming F, *et al*. Clinical efficacy of Xijiao Dihuang decoction combined with conventional treatment on acute cerebral infarction patients with stasis heat syndrome and its impact on blood lipid levels. *Prog Mod Biomed*. 2024;24(8):1495-1499.

   doi: 10.13241/j.cnki.pmb.2024.08.018

9. Hao S. *Effect of Xijiao Dihuang Decoction on Autophagy Level and its Regulatory Mechanism in Rats with Focal Lschemia Reperfusion*. Nanjing: Nanjing University of Chinese Medicine; 2019.

10. Eckner R, Ewen ME, Newsome D, *et al*. Molecular cloning and functional analysis of the adenovirus E1A-associated 300-kD protein (p300) reveals a protein with properties of a transcriptional adaptor. *Genes Dev*. 1994;8(8):869-884.

    doi: 10.1101/gad.8.8.869

11. Gronkowska K, Robaszkiewicz A. Genetic dysregulation of EP300 in cancers in light of cancer epigenome control - targeting of p300-proficient and -deficient cancers. *Mol Ther Oncol*. 2024;32(4):200871.

doi: 10.1016/j.omton.2024.200871

12. Rubio K, Molina-Herrera A, Perez-Gonzalez A, *et al*. EP300 as a molecular integrator of fibrotic transcriptional programs. *Int J Mol Sci*. 2023;24(15):12302.

doi: 10.3390/ijms241512302

13. Durbin AD, Wang T, Wimalasena VK, *et al*. EP300 selectively controls the enhancer landscape of MYCN-amplified neuroblastoma. *Cancer Discov*. 2022;12(3):730-751.

doi: 10.1158/2159-8290.CD-21-0385

14. Yang H, Liu X, Zhu X, *et al*. CPVL promotes glioma progression via STAT1 pathway inhibition through interactions with the BTK/p300 axis. *JCI Insight*. 2021;6(24):e146362.

doi: 10.1172/jci.insight.146362

15. Hou W, Hao Y, Sun L, Zhao Y, Zheng X, Song L. The dual roles of autophagy and the GPCRs-mediating autophagy signaling pathway after cerebral ischemic stroke. *Mol Brain*. 2022;15(1):14.

doi: 10.1186/s13041-022-00899-7

16. Son SM, Park SJ, Stamatakou E, Vicinanza M, Menzies FM, Rubinsztein DC. Leucine regulates autophagy via acetylation of the mTORC1 component raptor. *Nat Commun*. 2020;11(1):3148.

doi: 10.1038/s41467-020-16886-2

17. Xu Y, Wan W. Emerging roles of p300/CBP in autophagy and autophagy-related human disorders. *J Cell Sci*. 2023;136(12):jcs261028.

doi: 10.1242/jcs.261028

18. Peng L, Hu G, Yao Q, *et al*. Microglia autophagy in ischemic stroke: A double-edged sword. *Front Immunol*. 2022;13:1013311.

doi: 10.3389/fimmu.2022.1013311

19. Mo Y, Sun YY, Liu KY. Autophagy and inflammation in ischemic stroke. *Neural Regen Res*. 2020;15(8):1388-1396.

doi: 10.4103/1673-5374.274331

20. Sebti S, Prebois C, Perez-Gracia E, *et al*. BAG6/BAT3 modulates autophagy by affecting EP300/p300 intracellular localization. *Autophagy*. 2014;10(7):1341-1342.

doi: 10.4161/auto.28979

21. Kumar S, Gu Y, Abudu YP, *et al*. Phosphorylation of syntaxin 17 by TBK1 controls autophagy initiation. *Dev Cell*. 2019;49(1):130-144.e6.

doi: 10.1016/j.devcel.2019.01.027

22. Shen Q, Shi Y, Liu J, *et al*. Acetylation of STX17 (syntaxin 17) controls autophagosome maturation. *Autophagy*. 2021;17(5):1157-1169.

doi: 10.1080/15548627.2020.1752471

23. Pietrocola F, Castoldi F, Markaki M, *et al*. Aspirin recapitulates features of caloric restriction. *Cell Rep*. 2018;22(9):2395-2407.

doi: 10.1016/j.celrep.2018.02.024

24. Lei L, Lu Q, Ma G, Li T, Deng J, Li W. P53 protein and the diseases in central nervous system. *Front Genet*. 2022;13:1051395.

doi: 10.3389/fgene.2022.1051395

25. Ito A, Lai CH, Zhao X, *et al*. P300/CBP-mediated p53 acetylation is commonly induced by p53-activating agents and inhibited by MDM2. *EMBO J*. 2001;20(6):1331-1340.

doi: 10.1093/emboj/20.6.1331

26. Xue Y, Zeng X, Tu WJ, Zhao J. Tumor necrosis factor- α: The next marker of stroke. *Dis Markers*. 2022;2022:2395269.

doi: 10.1155/2022/2395269

27. Doll DN, Barr TL, Simpkins JW. Cytokines: Their role in stroke and potential use as biomarkers and therapeutic targets. *Aging Dis*. 2014;5(5):294-306.

doi: 10.14336/AD.2014.0500294

28. Mukherjee SP, Behar M, Birnbaum HA, Hoffmann A, Wright PE, Ghosh G. Analysis of the RelA: CBP/p300 interaction reveals its involvement in NF-κB-driven transcription. *PLoS Biol*. 2013;11(9):e1001647.

doi: 10.1371/journal.pbio.1001647

29. Sha JY, Zhou YD, Yang JY, *et al*. Maltol (3-Hydroxy-2-methyl-4-pyrone) slows d-galactose-induced brain aging process by damping the Nrf2/HO-1-mediated oxidative stress in mice. *J Agric Food Chem*. 2019;67(37):10342-10351.

doi: 10.1021/acs.jafc.9b04614

30. Lu H, Fu C, Kong S, *et al*. Maltol prevents the progression of osteoarthritis by targeting PI3K/Akt/NF-κB pathway: *In vitro* and *in vivo* studies. *J Cell Mol Med*. 2021;25(1):499-509.

doi: 10.1111/jcmm.16104

31. Wang WT, Fan ML, Hu JN, *et al*. Maltol, a naturally occurring flavor enhancer, ameliorates cisplatin-induced apoptosis by inhibiting NLRP3 inflammasome activation by modulating ROS-mediated oxidative stress. *J Funct Foods*. 2022;94:105127.

doi: 10.1016/j.jff.2022.105127

32. Bai D, Ueno L, Vogt PK. Akt-mediated regulation of NFkappaB and the essentialness of NFkappaB for the oncogenicity of PI3K and akt. *Int J Cancer*. 2009;125(12):2863-2870.

doi: 10.1002/ijc.24748

33. Zhou XY, Dai HY, Zhang H, Zhu JL, Hu H. Signal transducer and activator of transcription family is a prognostic marker associated with immune infiltration in endometrial cancer. *J Clin Lab Anal*. 2022;36(4):e24315.

doi: 10.1002/jcla.24315

34. Wang S, Awad KS, Elinoff JM, *et al*. G protein-coupled receptor 40 (GPR40) and peroxisome proliferator-activated receptor γ (PPARγ): AN integrated two-receptor signaling pathway. *J Biol Chem*. 2015;290(32):19544-19557.

doi: 10.1074/jbc.M115.638924

35. Ahn H, Lee G, Han BC, Lee SH, Lee GS. Maltol, a natural flavor enhancer, inhibits NLRP3 and non-canonical inflammasome activation. *Antioxidants (Basel)*. 2022;11(10):1923.

doi: 10.3390/antiox11101923

36. Jin MH, Hu JN, Zhang M, *et al*. Corrigendum to 'maltol attenuates polystyrene nanoplastic-induced enterotoxicity by promoting AMPK/mTOR/TFEB-mediated autophagy and modulating gut microbiota' [Environmental pollution, maltol attenuates polystyrene nanoplastic-induced enterotoxicity by promoting AMPK/mTOR/TFEB-mediated autophagy and modulating gut microbiota, volume 322 (2023), 121202]. *Environ Pollut*. 2023;334:122127.

doi: 10.1016/j.envpol.2023.122127

37. Gu M, Su ZG, Janson JC. One-step purification of 3,4-dihydroxyphenyllactic acid, salvianolic acid B, and protocatechualdehyde from salvia miltiorrhiza bunge by isocratic stepwise hydrogen bond adsorption chromatography on cross-linked 12% agarose. *J Chromatogr Sci*. 2008;46(2):165-168.

doi: 10.1093/chromsci/46.2.165

38. Cao S, Chen S, Qiao X, *et al*. Protocatechualdehyde rescues oxygen-glucose deprivation/reoxygenation-induced endothelial cells injury by inducing autophagy and inhibiting apoptosis via regulation of SIRT1. *Front Pharmacol*. 2022;13:846513.

doi: 10.3389/fphar.2022.846513

39. Bouras T, Fu M, Sauve AA, *et al*. SIRT1 deacetylation and repression of p300 involves lysine residues 1020/1024 within the cell cycle regulatory domain 1. *J Biol Chem*. 2005;280(11):10264-10276.

doi: 10.1074/jbc.M408748200

40. Guo Y, Yang JH, He Y, *et al*. Protocatechuic aldehyde prevents ischemic injury by attenuating brain microvascular endothelial cell pyroptosis via lncRNA Xist. *Phytomedicine*. 2022;94:153849.

doi: 10.1016/j.phymed.2021.153849

41. He M, Chiang HH, Luo H, *et al*. An acetylation switch of the NLRP3 inflammasome regulates aging-associated chronic inflammation and insulin resistance. *Cell Metab*. 2020;31(3):580-591.e5.

doi: 10.1016/j.cmet.2020.01.009

42. Zhang T, Ma C, Zhang Z, Zhang H, Hu H. NF-κB signaling in inflammation and cancer. *Med Comm (2020)*. 2021;2(4):618-653.

doi: 10.1002/mco2.104

43. Winter AN, Brenner MC, Punessen N, *et al*. Comparison of the neuroprotective and anti-inflammatory effects of the anthocyanin metabolites, protocatechuic acid and 4-hydroxybenzoic acid. *Oxid Med Cell Longev*. 2017;2017:6297080.

doi: 10.1155/2017/6297080

44. Kong BS, Cho YH, Lee EJ. G protein-coupled estrogen receptor-1 is involved in the protective effect of protocatechuic aldehyde against endothelial dysfunction. *PLoS One*. 2014;9(11):e113242.

doi: 10.1371/journal.pone.0113242

45. Zeng M, Shao C, Zhou H, *et al*. Protocatechudehyde improves mitochondrial energy metabolism through the HIF1α/PDK1 signaling pathway to mitigate ischemic stroke-elicited internal capsule injury. *J Ethnopharmacol*. 2021;277:114232.

doi: 10.1016/j.jep.2021.114232

46. Bolun Z, Guannan Z. Advances in the treatment of advanced melanoma with NRAS gene mutation. *China Oncol*. 2023;33(10):936-944.

doi: 10.19401/j.cnki.1007-3639.2023.10.006

47. Randic T, Kozar I, Margue C, Utikal J, Kreis S. NRAS mutant melanoma: Towards better therapies. *Cancer Treat Rev*. 2021;99:102238.

doi: 10.1016/j.ctrv.2021.102238

48. Wang J, Liu Y, Li Z, *et al*. Endogenous oncogenic nras mutation initiates hematopoietic malignancies in a dose- and cell type-dependent manner. *Blood*. 2011;118(2):368-379.

doi: 10.1182/blood-2010-12-326058

49. Valencia-Sama I, Ladumor Y, Kee L, *et al*. NRAS status determines sensitivity to SHP2 inhibitor combination therapies targeting the RAS-MAPK pathway in neuroblastoma. *Cancer Res*. 2020;80(16):3413-3423.

doi: 10.1158/0008-5472.CAN-19-3822

50. Kuiming Z, Yinglin C, Luandie G, *et al*. Research progress in effect of p38 MAPK signal pathway on ischemic stroke. *Med Recapitulate*. 2021;27(09):1691-1695.

51. Meng-Yang J. The role of p38 MAPK- PPARγ/NF-κB signaling pathway inthe induction of brain ischemic tolerance induced bycerebral ischemic preconditioning. Hebei Medical University. 2014.

52. Zhang B, Wei YZ, Wang GQ, Li DD, Shi JS, Zhang F. Targeting MAPK pathways by naringenin modulates microglia M1/M2 polarization in lipopolysaccharide-stimulated cultures. *Front Cell Neurosci*. 2018;12:531.

doi: 10.3389/fncel.2018.00531

53. Chen MJ, Ramesha S, Weinstock LD, *et al*. Extracellular

signal-regulated kinase regulates microglial immune responses in Alzheimer's disease. *J Neurosci Res*. 2021;99(6):1704-1721.

doi: 10.1002/jnr.24829

54. Vu HL, Aplin AE. Targeting mutant NRAS signaling pathways in melanoma. *Pharmacol Res*. 2016;107:111-116.

doi: 10.1016/j.phrs.2016.03.007

55. Chu E, Mychasiuk R, Hibbs ML, Semple BD. Dysregulated phosphoinositide 3-kinase signaling in microglia: Shaping chronic neuroinflammation. *J Neuroinflammation*. 2021;18(1):276.

doi: 10.1186/s12974-021-02325-6

56. Xin-Yu HU, Xue W, Wen-Qian LU, *et al*. Involvement of mitochondria-mediated pathway and akt/GSK3β signaling in protective action of albiflorin against MPP~+-induced PC12 cells apoptosis. *Chin Pharm J*. 2016;51(17):1467-1471.

doi: 10.11669/cpj.2016.17.007

57. Yoeli-Lerner M, Chin YR, Hansen CK, Toker A. Akt/protein kinase b and glycogen synthase kinase-3beta signaling pathway regulates cell migration through the NFAT1 transcription factor. *Mol Cancer Res*. 2009;7(3):425-432.

doi: 10.1158/1541-7786.MCR-08-0342

58. Palanivel C, Chaudhary N, Seshacharyulu P, *et al*. The GSK3 kinase and LZTR1 protein regulate the stability of ras family proteins and the proliferation of pancreatic cancer cells. *Neoplasia*. 2022;25:28-40.

doi: 10.1016/j.neo.2022.01.002

59. Oh YJ, Jin SE, Shin HK, Ha H. Daeshiho-tang attenuates inflammatory response and oxidative stress in LPS-stimulated macrophages by regulating TLR4/MyD88, NF-κB, MAPK, and Nrf2/HO-1 pathways. *Sci Rep*. 2023;13(1):18891.

doi: 10.1038/s41598-023-46033-y

60. Zhang H, Wang J, Lang W, *et al*. Albiflorin ameliorates inflammation and oxidative stress by regulating the NF-κB/NLRP3 pathway in methotrexate-induced enteritis. *Int Immunopharmacol*. 2022;109:108824.

doi: 10.1016/j.intimp.2022.108824

61. Ou Z, Li P, Wu L, *et al*. Albiflorin alleviates neuroinflammation of rats after MCAO via PGK1/Nrf2/HO-1 signaling pathway. *Int Immunopharmacol*. 2024;137:112439.

doi: 10.1016/j.intimp.2024.112439

62. Kryszczuk M, Kowalczuk O. Significance of NRF2 in physiological and pathological conditions an comprehensive review. *Arch Biochem Biophys*. 2022;730:109417.

doi: 10.1016/j.abb.2022.109417

63. Banerjee N, Wang H, Wang G, Boor PJ, Khan MF. Redox-sensitive Nrf2 and MAPK signaling pathways contribute to trichloroethene-mediated autoimmune disease progression. *Toxicology*. 2021;457:152804.

doi: 10.1016/j.tox.2021.152804

64. Ferro E, Goitre L, Retta SF, Trabalzini L. The interplay between ROS and ras GTPases: physiological and pathological implications. *J Signal Transduct*. 2012;2012:365769.

doi: 10.1155/2012/365769

65. Zhang L, Xu J, Yin S, Wang Q, Jia Z, Wen T. Albiflorin attenuates neuroinflammation and improves functional recovery after spinal cord injury through regulating LSD1-mediated microglial activation and ferroptosis. *Inflammation*. 2024;47(4):1313-1327.

doi: 10.1007/s10753-024-01978-8

66. Sun S, Jimu RB, Lema AK, *et al*. A systematic review on the origin, anti-inflammatory effect, mechanism, pharmacokinetics, and toxicity of albiflorin. *Arab J Chem*. 2024;17(7):105836.

doi: 10.1016/j.arabjc.2024.105836

67. Zhou J, Wang L, Wang J, *et al*. Paeoniflorin and albiflorin attenuate neuropathic pain via MAPK pathway in chronic constriction injury rats. *Evid Based Complement Alternat Med*. 2016;2016:8082753.

doi: 10.1155/2016/8082753